Remote Sensing of Environment 262 (2021) 112482

Contents lists available at ScienceDirect

Remote Sensing of Environment

journal homepage: www.elsevier.com/locate/rse

Review

Remote sensing of sun-induced chlorophyll-*a* fluorescence in inland and coastal waters: Current state and future prospects

Remika S. Gupana [a,b,*], Daniel Odermatt [a,b], Ilaria Cesana [c], Claudia Giardino [d], Ladislav Nedbal [e], Alexander Damm [a,b]

[a] Eawag, Swiss Federal Institute of Aquatic Science & Technology, Surface Waters – Research and Management, Überlandstrasse 133, 8600 Dübendorf, Switzerland
[b] Department of Geography, University of Zurich, Winterthurerstrasse 190, 8057 Zurich, Switzerland
[c] Remote Sensing of Environmental Dynamics Laboratory, DISAT, University of Milano-Bicocca, Piazza della Scienza 1, 20126 Milan, Italy
[d] Institute for Electromagnetic Sensing of the Environment, National Research Council (CNR-IREA), Via Bassini 15, 20133, Milan, Italy
[e] Institute of Bio- and Geosciences/Plant Sciences (IBG-2), Forschungszentrum Jülich, Wilhelm-Johnen-Straße, D-52428 Jülich, Germany

ARTICLE INFO

Editor: Dr. Menghua Wang.

Keywords:
Phytoplankton fluorescence
Optically complex waters
Case-2 waters
Hyperspectral data
Phytoplankton remote sensing
Water quality
Review

ABSTRACT

Sun-induced fluorescence (SIF) retrieved from satellite measurements has been widely used as proxy for chlorophyll-*a* concentration and as indicator of phytoplankton physiological status in oceans. The practical use of this naturally occurring light signal in environmental research is, however, under-exploited, particularly in research focusing on optically complex waters such as inland and coastal waters. In this study, we investigated methodological and knowledge gaps in remote sensing of chlorophyll-*a* SIF in optically complex waters by reviewing the theory behind SIF occurrence, the availability of existing and upcoming instrumentation, the availability of SIF retrieval schemes, and the applications for aquatic research.

Starting with an overview of factors that influence SIF leaving the water body, we further investigated available and upcoming observational capacity by in situ, airborne and satellite sensors. We discuss requirements for spatial, spectral, temporal, and radiometric resolution of observing systems in the context of SIF dynamics. We assessed viable retrieval techniques able to disentangle SIF from non-SIF contribution to the upwelling radiance, ranging from the established multispectral Fluorescence Line Height algorithm (FLH) approach to hyperspectral approaches including model inversion, spectral fitting methods and machine learning regression procedures. Finally, we provide an overview of applications, which could potentially benefit from improved SIF emission estimates such as biomass estimation, algal bloom investigation and primary productivity modelling.

1. Introduction

Sun-induced fluorescence (SIF) emission from chlorophyll *a* (chl *a*) pigments in phytoplankton is a convenient reporter signal of phytoplankton biomass and primary productivity in aquatic environments (Falkowski and Kiefer, 1985). Particularly for inland or coastal waters, measurements of phytoplankton SIF are beneficial for monitoring water quality due to the dynamic nature of such environments and their often intensively used shores (Mouw et al., 2015; Muller-Karger et al., 2018). Large scale, high frequency and synoptic monitoring of SIF is facilitated by satellite remote sensing (RS). Particularly, medium resolution, wide-swath sensors such as MODIS, MERIS and OLCI, in combination with the Fluorescence Line Height (FLH) method (e.g. Gower et al., 1999; Letelier and Abbott, 1996) have been widely used for estimates of phytoplankton SIF (Gilerson et al., 2008; Gower and Borstad, 2004; Hu et al., 2005).

Chl-*a* fluorescence emission occurs with a quantum yield that does not exceed few percent of the absorbed light (Zhou et al., 2008). This emitted signal is characterized by an emission peak at 685 nm (λ_{em}) (IOCCG, 2000) that adds to other upwelling radiance components, resulting in a total top of atmosphere radiance signal ($L_{TOA}(\lambda_{em})$) when detected by a satellite sensor:

$$L_{TOA}(\lambda_{em}) = L_a(\lambda_{em}) + L_e(\lambda_{em}) + L_r(\lambda_{em}) + SIF(\lambda_{em}) \quad (1)$$

where L_a corresponds to path scattered radiance, L_e to upwelling elastic scattering, L_r to specular reflected radiance, while the latter two are modulated by atmospheric transmission. For water bodies close to a

* Corresponding author at: Eawag, Swiss Federal Institute of Aquatic Science & Technology, Surface Waters – Research and Management, Überlandstrasse 133, 8600 Dübendorf, Switzerland
E-mail address: remika.gupana@eawag.ch (R.S. Gupana).

https://doi.org/10.1016/j.rse.2021.112482
Received 7 December 2020; Received in revised form 8 April 2021; Accepted 28 April 2021
Available online 21 May 2021

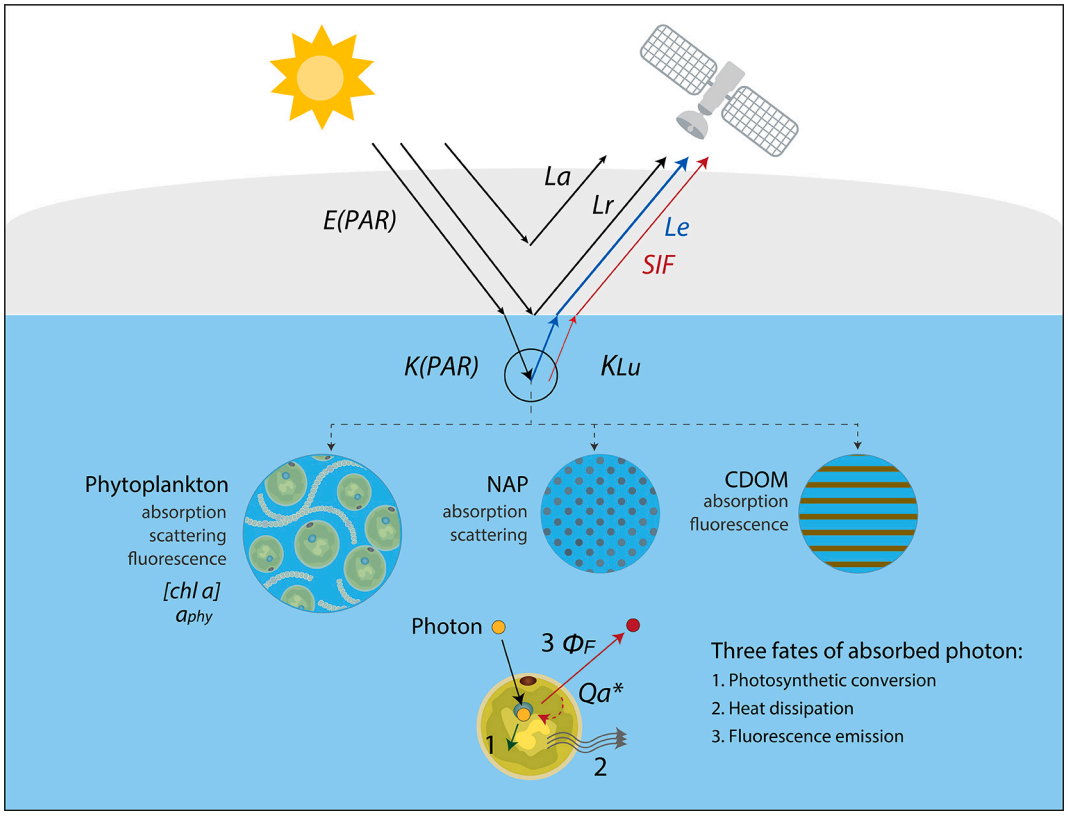

Fig. 1. Schematic of components contributing to total upwelling radiance measured by a sensor with emphasis on fluorescence. Phytoplankton figure adapted from Integration and Application Network (ian.umces.edu/media-library - CC BY-SA 4.0) and other vector symbols from vecteezy.com

terrestrial area (heterogeneous landscapes), contribution of adjacency effects to the total upwelling radiance should also be considered (Frouin et al., 2019). Satellite-based SIF retrievals require disentangling SIF from other radiance components. This task is challenging since SIF itself is a function of environmental factors (i.e. light availability, water temperature) (Popik and Gamayunov, 2015), phytoplankton characteristics (e.g. light harvesting, physiology), path modulation (i.e. intercellular, in the water body, in the atmosphere), sensor characteristics, and retrieval schemes (Huot and Babin, 2010).

Optically complex waters, typically found in inland and coastal waters, contain independently varying concentrations of chl-a mainly attributed to phytoplankton, total suspended matter (TSM) and colored dissolved organic matter (CDOM). The variability of inherent optical properties (IOPs) related to these components further complicates the retrieval of SIF (IOCCG, 2000). FLH, for example, exploits only three bands in the red and near infrared region, which leaves the discrimination of elastic and inelastic signal contributions inaccurate in a wide range of water types and impairs SIF retrievals in lakes and coastal areas (Gilerson et al., 2008). High-resolution imaging spectrometers (hyperspectral sensors) provide hundreds of spectral bands to better determine the different optical components' signal contributions. However, the efficacy of this improvement for SIF retrieval is still an open topic and needs further investigation.

This study aims to provide a thorough review of RS of phytoplankton SIF in optically complex waters by re-examining factors that contribute to SIF emissions, availability of instrumentation and retrieval methods, and applications for aquatic research. We analyze gaps and challenges in SIF RS and finally, how future satellite missions could alleviate present limitations. This review complements previous reviews concerning Earth observation of aquatic ecosystems, water constituent retrieval in optically complex waters (Matthews, 2011; Odermatt et al., 2012), phytoplankton bloom detection (Blondeau-Patissier et al., 2014; Kutser, 2009), satellite mission requirements (Mouw et al., 2015; CEOS, 2018), and bio-optical modelling of phytoplankton SIF (Gilerson and Huot, 2017).

2. Principles and origin of SIF emissions in aquatic systems

Various components determine water leaving SIF emissions, including photon flux and light harvesting, phytoplankton physiology and factors causing path modulations (Fig. 1).

Following Babin et al., 1996; Gordon, 1979; Maritorena et al., 2000, the upwelling water leaving SIF and all components (i.e. instrumentation, light harvesting, physiology, path modulation) contributing to the retrieved SIF signal for a given sensor depth z and distance of the sensor to a thin water layer x can be mathematically represented as:

$$dSIF(z) = \left(\frac{1}{4\pi}\right) \cdot E(PAR, z)\left(e^{-K(PAR)x}\right)[chl\ a]\,\overline{a}^{*}_{\phi}\,\phi_F\,Q^{*}_{a}\left(e^{-K_{Lu}(\lambda_{em})x}\right)dx \quad (2)$$

The light harvesting component is comprised of the parameters $E(PAR)$, the scalar irradiance integrated from 400 nm to 700 nm; $K(PAR)$, the attenuation coefficient in the excitation irradiance; $[chl\ a]$, the chl a concentration; and $\overline{a}^{*}_{\phi}$,the irradiance-weighted chl-a-specific absorption coefficient of phytoplankton. The physiological component is comprised of ϕ_F,the fluorescence quantum yield. Lastly, the parameters constituting path modulation are Q_a*,the intracellular reabsorption of fluorescence, and $K_{Lu}(\lambda_{em})$, the attenuation coefficient for upwelling

radiance. The fraction of isotropic fluorescence emission per solid angle unit is given by the factor $1/4\pi$. We assume that [*chl a*], $\bar{a}_{\phi}^{*}$, ϕ_F, and Q_a* are invariant across all euphotic depths, and that the water depth exceeds the euphotic depth. Main components determining Eq. 2 are further explained in the following chapters. Integrating Eq. 2 over x from 0 to ∞ will allows expressing water leaving SIF as:

$$SIF(z) = \frac{\dot{E}(PAR, z)[chl\ a]\ \bar{a}_{\phi}^{*}\ \phi_F\ Q_a^{*}}{4\pi\ (K(PAR) + K_{Lu}(\lambda_{em}))} \quad (3)$$

2.1. Light harvesting from E_d to phytoplankton chl-a

$\dot{E}(PAR)$ is the potentially available energy that is partly emitted as fluorescence light, while various processes alter the energy transfer between both, upwelling and downwelling radiance components. Incident $\dot{E}(PAR)$ is partially attenuated (coefficient symbolized by $K(PAR)$) before it is partly absorbed by pigment molecules embedded in phytoplankton. Consequently, knowledge of $\dot{E}(PAR)$ and its spatio-temporal dynamics is pivotal for reliable estimates and interpretation of SIF (Xing et al., 2007).

The planktonic [chl *a*] determines the amount of incident energy which can be absorbed by photosynthetic pigments and thus affects SIF emissions (Huot and Babin, 2010). This mechanistic dependency inspired several studies relating SIF to aquatic biomass in coastal areas and lakes (e.g. Gons et al., 2008; Gower and King, 2007; Gower et al., 1999). Ample evidence, however, indicates limitation of this approach under conditions with high $\dot{E}(PAR)$ when phytoplankton adapt to reduce photodamage, leading to divergence in the proportionality between phytoplankton biomass (chl *a*) and SIF (Behrenfeld et al., 2009; Graff and Behrenfeld, 2018) (see Section 2.2).

The specific absorption coefficient of phytoplankton $\bar{a}_{\phi}^{*}$ is a fundamental index of chl *a* absorption. Variabilities in the magnitude of $\bar{a}_{\phi}^{*}$ are due to packaging effects in chl-*a* pigments as function of changing irradiance and phytoplankton cell size (Fujiki and Taguchi, 2002).

2.2. Physiology

The amount of light absorbed by planktonic chl-a is equivalent to the product of attenuated $\dot{E}(PAR)$, [chl *a*] and $\bar{a}_{\phi}^{*}$. The fraction of absorbed light which is emitted as SIF is the fluorescence quantum yield (ϕ_F). This ϕ_F is better referred to as effective ϕ_F to inherently account for energy absorbed by non-photosynthetic pigments (Gilerson and Huot, 2017). Accessory pigments such as phycocyanin and phycoerythrin also emit fluorescence in shorter wavelength regions (IOCCG, 2014) but are beyond the scope of this review. However, a fraction of the light absorbed by the accessory pigments is distributed to chl *a* and subsequently, emitted as fluorescence in the chl *a* emission region (Millie et al., 2002; Simis and Huot, 2012).

Absorbed light energy can have different fates within the phytoplankton: 1) charge separation in the reaction centers of Photosystem II and Photosystem I (PS I) leading to photochemistry, 2) SIF emission and 3) heat dissipation. The occurrence of the three fates depends on energy quenching mechanisms undergone by the phytoplankton. In both photochemical quenching (PQ) and non-photochemical quenching (NPQ) conditions, energy available for SIF emission is reduced but attributed to different causes. High PQ signals lead to high quantum yield of photochemistry and low heat dissipation, while NPQ increases heat dissipation and reduces energy supply to the reaction centers and, thus, photosynthetic energy conversion. The photoprotective NPQ mechanism is activated as a reaction to high light conditions and leads to a reduction of photons available for both photosynthesis and SIF (Gilerson and Huot, 2017). Changes in SIF due to NPQ are particularly apparent during a few hours at and near solar noon on bright and clear days (Poulin et al., 2018; Roesler and Barnard, 2013). By estimating a NPQ-corrected ϕ_F associated to a retrieved SIF signal (Behrenfeld et al., 2009), one can gain insight into photosynthetic processes during PQ. ϕ_F is therefore not only important in quantifying SIF but also in quantifying primary productivity (Huot and Babin, 2010).

2.3. Path modulation

The entire SIF radiation emitted at the molecular level cannot all be detected at cellular or community level. Part of emitted SIF is reabsorbed by the cells due to the spectral overlap of pigment absorption and emission wavelengths. This intracellular reabsorption factor is denoted as Q_a* (Collins et al., 1985; Huot and Babin, 2010). From the cellular level, emitted SIF is attenuated as it travels from the cell upwards to the water surface. This interaction is referred to as attenuation of upwelling radiance (K_{Lu}). Although sometimes approximated with total absorption (e.g. Huot and Babin, 2010; Maritorena et al., 2000), a more encompassing K_{Lu} notation is preferred for optically complex waters.

Raman scattering, a form of inelastic scattering, may contribute 25–35% of total E_u at depths below 63 m in open ocean waters (Maritorena et al., 2000) but is typically negligible for measurements close to the surface (Frouin et al., 2008; Huot and Babin, 2010). The possible contribution of Raman scattering at 685 nm in areas with low phytoplankton biomass is due to excitation at 555 nm (Morrison, 2003). The relative contribution of Raman scattering to upwelling radiance decreases in the red spectral region with increasing chl-*a* absorption or particle scattering (Bismarck and Fischer, 2013). As a rule of thumb, Raman scattering is non-negligible in oligotrophic conditions (i.e. [chl *a*] < 1 mg m^{-3}) (Morel et al., 2002).

2.4. Impact of in-water constituent concentration to SIF signal

The SIF signal is affected by attenuation in the downwelling and upwelling radiance fields, represented by K(PAR) and $K(L_u)$ (cf. Eq. (2)), respectively. Attenuation depends on absorption and scattering of light and consequently, on in-water constituent concentrations. The magnitude of attenuation therefore significantly determines the extent of water depth observable via above-water or TOA RS.

CDOM absorption is prominent in the blue wavelength region that is distinct from the SIF emission band centered at 685 nm and, therefore, less relevant for SIF retrievals (e.g. Doerffer, 1993; Hu and Feng, 2016). However, if CDOM concentration is high, it attenuates $\dot{E}(PAR)$ and upwelling radiance to a level that makes the retrieval of SIF virtually impossible (Kutser et al., 2016). Similar to CDOM, high concentrations of non-algal particles (NAP) may limit light availability and thus reduces the absolute radiance flux absorbed by phytoplankton (Gilerson et al., 2007). Subsequently, absorption and backscattering due to NAP along with CDOM absorption resulted in a substantially lower SIF emission for a given [chl *a*] compared to same [chl *a*] in oceanic waters (Gilerson et al., 2007).

In low [chl *a*] waters, the peak near 685 nm apparent in upwelling radiance is attributed to [chl-*a*] fluorescence (Gordon, 1979) following the assumption that the contribution of elastic scattering to the upwelling photon flux (L_e) is negligible relative to the SIF emission peak at 685 nm. However, in cases where [chl *a*] and TSM are high, the

reflectance peak shifts to longer wavelengths, moving up to 25 nm (Gilerson et al., 2008; Schalles, 2006). This apparent shift is due to the combination of pigment absorption at <700 nm and particle backscattering dominance resulting in an increased reflectance at around 700 nm until water absorption becomes more pronounced at 710 nm (Gilerson et al., 2007). The roughly sigmoidal increase in pure water absorption between 700 and 740 nm limits the reflectance peak to shift to even longer wavelengths. The shift in peak reflectance towards NIR of productive ecosystems has been also observed in cyanobacteria-dominated waters (Moore et al., 2017; Palmer et al., 2015; Stumpf et al., 2012) where chl-*a* fluorescence is superimposed by high elastic scattering e.g. from gas vacuoles in *Microcystis aeruginosa* (Matthews and Bernard, 2013).

3. Suitability of observational systems to measure SIF dynamics

The water-leaving radiance comprising SIF and scattered radiance can be measured with a variety of in-situ, airborne and spaceborne spectrometers. Spaceborne instrument requirements for ocean color RS (IOCCG, 2012, 1998; Muller-Karger et al., 2018) and RS of optically complex waters (CEOS, 2018; Mouw et al., 2015) have been assessed in previous studies. This section provides a complementary assessment of SIF-specific instrumental requirements in terms of spatial, temporal, spectral, and radiometric resolution. We also evaluate available and upcoming across scale sensor systems concerning identified requirements and their suitability to measure SIF.

3.1. SIF dynamics and sensor requirements

3.1.1. Spatial resolution

The spatial resolution required for SIF RS depends on the geometry of selected water bodies and the spatial scale of their relevant bio-optical gradients. This impedes defining a unique spatial resolution across applications. Since similar thinking for optically deep complex waters can be used to indicate suitable spatial dynamics required to map SIF dynamics, the following bulk indications can be followed. For areas up to 200 m from the shore that are characterized by well-mixed conditions, the suggested spatial resolution ranges between 100 m (Bissett et al., 2004) and 250–300 m IOCCG (2012). Areas within and adjacent to river plumes encounter dynamic dispersion of water constituents, necessitating a large range of resolutions between 30 m – 1 km (IOCCG, 2000). For specific applications such as harmful algal bloom or aquaculture monitoring, a high spatial resolution of around 30–50 m is suggested (IOCCG, 2012, 2000). Using area as basis for spatial resolution requirement, CEOS (2018) defines 333 m as acceptable for areas $\geq$1 km^2, while a resolution between ~17 and ~ 33 m is a general recommendation for applicability in a wide variety of inland and coastal water bodies. Trivial but true, the spatial resolution must fit the underlying process dynamic, which requires finer resolution in areas with spatially heterogeneous distribution of water constituents and vice versa (Mouw et al., 2015).

3.1.2. Temporal resolution

Phytoplankton SIF emissions vary in time due to complex dependencies described in Section 2. Available polar-orbiting satellites can adequately monitor resulting seasonal variations in SIF, a capacity especially important during bloom events and for primary productivity estimates. But polar-orbiting satellites are unable to resolve diurnal SIF dynamics. Geostationary satellites such as the multispectral Geostationary Ocean Color Imager (GOCI) generates images of the Korean peninsula eight times a day, which enables the monitoring of phytoplankton fluorescence diel cycles, photophysiology and abrupt changes in biomass and primary productivity (Lee et al., 2012; O'Malley et al., 2014). Other sub-diel processes in optically complex waters are likely to impact SIF measurements, such as shifting tides, changing cloud cover and varying discharges from point sources (Mouw et al., 2015; Tzortziou et al., 2015). An important consideration is that satellites have repeat cycles which are typically inversely proportional to spatial resolution (CEOS, 2018; Groom et al., 2019). This causes an important trade-off between spatial and temporal resolution that must be assessed depending on the desired SIF application.

3.1.3. Spectral resolution

Robust SIF estimates rely on radiometric measurements in a suitable number of bands with a suitable bandwidth. Particularly, two aspects determine this resolution, SIF emission characteristics and requirements defined by the underlying SIF retrieval method.

Chlorophyll SIF emission spectra are well defined with theoretically two emission peaks at 685 nm and 740 nm (Mohammed et al., 2019). Due to strong water absorption, only the first peak dominates apparent phytoplankton SIF while the second peak is almost completely diminished. A proper sampling of the emission shape requires a spectral resolution that allows resolving shape and position of the signal. Furthermore, disentangling emitted SIF and reflected radiance in conditions encompassing a wide range of optically active constituent requires spectrally contrasting information achievable with high spectral resolution in the SIF emission region and in spectral regions with significant absorption and scattering due to phytoplankton, CDOM and NAP (Mouw et al., 2015). The definition of spectral requirements is further complicated by needs of the employed SIF retrieval scheme. So far, there is no consensus about appropriate spectral resolution for SIF retrievals in optically complex waters. Existing recommendations for medium resolution ocean color spectrometers suggest a spectral bandwidth (full width half maximum, FWHM) of 5 to 8 nm (CEOS, 2018) or 10 nm (IOCCG, 2012) around the fluorescence emission peak (~685 nm). Considering hyperspectral capability, successful demonstrations of SIF retrieval in optically complex waters through inversion techniques were based on simulations with 1 nm spectral resolution (Gilerson et al., 2007; Gilerson and Huot, 2017), and field measurements with bandwidths ranging from ~0.3 nm (Gilerson et al., 2007) to 10 nm (Huot et al., 2007). Approaches based on exploiting the atmospheric O_2-B absorption band require very high spectral resolution to effectively disentangle SIF from reflected radiances (Frouin et al., 2008), whereas other techniques such as FLH can be implemented at a relatively lower spectral resolution (Abbott and Letelier, 1996).

Spectral coverage is also important to provide critical context information for successful SIF retrievals and interpretation. Information about other water constituents and IOPs are, for example, critical to constrain elastic reflectance contributions and to understand phytoplankton traits that contribute to SIF emission. Due to sensitivity and saturation constraints, the wavelengths most suited for retrieving these constituents depend on concentration levels, and extend across the entire visible to NIR spectrum (Odermatt et al., 2012). It even ranges from 380 nm to the short-wave infrared when taking into account the requirements for atmospheric correction (Ibrahim et al., 2019; IOCCG, 2000).

Spectral stability is essential since a shift of the spectral response directly causes errors in reflectance or SIF retrieval. It is pivotal to identify and compensate possible spectral shift effects to avoid complex artefacts in the data that can eventually challenge data interpretation (IOCCG, 2012). Monitoring and quantifying spectral shifts can be facilitated with optimized spectral band configurations that, for

example, cover prominent absorption features in adequate spectral resolution. The analysis of such features and their spectral dynamics per pixel and across sensor array is an efficient strategy to estimate shifts and incorporate them in subsequent retrieval schemes (IOCCG, 2012).

3.1.4. Radiometric resolution

SIF adds a relatively weak signal to the reflected radiance signal. Sensitive observational systems must provide a high signal-to-noise (SNR) ratio to ensure a low detection limit of this small signal (Babin et al., 1996; Gege and Dekker, 2020). The detection limit can be expressed as minimum signal of detection (MSD) and is calculated as radiance signal divided by the SNR values of spectral bands involved in the SIF retrieval (Abbott and Letelier, 1996). High SNR therefore enables low MSD values and thus the detection of even small SIF signals. Aside from SIF, high SNR is generally needed in RS of optically complex waters with SNR values similar to clear open ocean waters (IOCCG, 2000).

Enabling a high SNR goes along with various trade-offs. It is often at the cost of spectral and/or spatial resolution to ensure that a sufficient amount of energy is captured per measurement (Qi et al., 2017). There are also trade-offs between SNR and dynamic range. Due to technical limitations, higher SNR requirements are associated with increasing sensor sensitivity and thus decrease the dynamic range and the radiance saturation limit (Hu et al., 2012; Qi et al., 2017). This can complicate atmospheric correction since high SNR requirements in the NIR can cause signal saturation in very turbid water conditions (Mouw et al., 2015).

IOCCG (2012) recommends SNR values to be at least 1400 in the 678 nm SIF emission band, 1000 for other visible bands, 600 for NIR and 100–250 for SWIR bands. These values were derived from SeaWiFS data and may be adjusted based on sensor solar and viewing geometries. Qi et al. (2017) argue that minimum SNR requirements are 400 for VIS and 600 for NIR when considering higher spectral and spatial requirements, but does not refer specifically to SIF bands.

3.2. Instrumentation – past, current and future

3.2.1. In-situ sensors

Historically, SIF field measurements were mostly obtained using spectroradiometers designed for open ocean (e.g. Maritorena et al., 2000; Morrison, 2003), coastal (Gilerson et al., 2007, 2008; Huot, 2004; Huot et al., 2007) and lacustrine waters (Dall'Olmo and Gitelson, 2005; Gilerson and Huot, 2017). A summary of commonly used in-situ sensors operating both underwater and above-water are provided in the appendix (Table A1).

A study by Vabson et al. (2019) compared several spectroradiometers such as SeaPRISM, RAMSES, HyperOCR, and WISP-3. While spectral range, sampling interval and FWHM vary significantly between these spectrometers, their study indicates that radiance and irradiance measurements between the different instruments operated by different scientists were similar with a standard deviation of less than 1% after data harmonization. Besides spectrometers specifically developed for aquatic applications, the new Fluorescence Box (FloX) spectrometer system was recently tested for phytoplankton SIF measurements (Di Cicco et al., 2020). The FloX system was developed for terrestrial SIF applications and comprises one broadband and one high resolution spectrometer to retrieve both SIF peaks at 685 and 740 nm along with different vegetation traits (Mohammed et al., 2019).

3.2.2. Airborne sensors

Phytoplankton SIF was first observed from an airborne spectrometer by Neville and Gower (1977) over Saanich inlet in Vancouver, Canada. They noted a relationship between the observed line height (similar to FLH) and [chl *a*] near the water surface. This research led to the development of the Fluorescence Line Imager (FLI) in the 1980's, with specifications optimized for SIF measurements (Abbott and Letelier, 1996; Gower and Borstad, 1990). The seminal study by Gower and Borstad (1990) was the first demonstration of retrieving phytoplankton SIF from airborne RS imagery. Almost a decade after, the Compact Airborne Spectral Imager (CASI) was used to study SIF, absorption and scattering components around the SIF emission peak (Gower et al., 1999). FLI and CASI are both imaging spectrometers with a high spectral resolution covering the VIS to NIR range with a FHWM and a sampling interval at 2.6 and roughly 1.5 nm, respectively, while spectral binning was applied to achieve the required SNR (Gower et al., 1999; Gower and Borstad, 1990). The airborne campaigns in the 1980s–1990s prepared the ground for the retrieval of SIF from MODIS, MERIS and Sentinel-3 data in the following decades. Recently, the Portable Remote Imaging Spectrometer (PRISM) operated by NASA was used to derive SIF profiles over the Southern Ocean (Erickson et al., 2019). Several examples of airborne spectrometers are given in the appendix (Table A2).

Although SIF-focused airborne measurement activities are sparse over the past two decades, other airborne spectrometers were used for several RS applications in optically complex waters (Table A2). Some examples of airborne based RS applications are pigment concentration retrieval (Li et al., 2013), estimates of suspended particulate matter (Giardino et al., 2015), and assessments of phytoplankton functional types (Palacios et al., 2015).

From the terrestrial SIF perspective, Forschungzentrum Jülich and Specim Spectral Imaging Ltd. developed the HyPlant airborne imaging spectrometer (Rascher et al., 2015). Hyplant is the first airborne sensor developed specifically for full SIF emission retrievals and is the airborne demonstrator to the upcoming Fluorescence Explorer (FLEX) satellite mission (Mohammed et al., 2019). Besides a VIS-NIR spectrometer (DUAL module), Hyplant comprises a fluorescence spectrometer (FLUO module) with a FWHM of 0.25 nm in the SIF emission wavelength region. The SNR, however, is rather low (240) for the FLUO module, which could limit the applicability of HyPlant for optically complex waters. In a recent study, Hyplant has been tested for SIF retrievals in coastal areas (Di Cicco et al., 2020), while an overall performance assessment and tests in inland waters are still pending.

3.2.3. Spaceborne sensors

Most satellite based research on SIF in optically complex waters over the past two decades is based on ocean color sensors (e.g. MODIS, MERIS, and OLCI) in combination with the FLH algorithm (e.g. Gower and Borstad, 2004; Kravitz et al., 2020; Montes-Hugo et al., 2012). These studies mainly focused on SIF and its relation to [chl *a*], hence exploited SIF as proxy for phytoplankton biomass. FLH was additionally applied to evaluate phytoplankton phenology (Palmer et al., 2015) and to detect algal blooms (McKibben et al., 2012). Interestingly, MERIS FLH yielded a better bloom detection due to its 709 nm band compared to MODIS which lacks this spectral channel (Gower and King, 2012; Zhao et al., 2010). The quantum yield of SIF was also determined from MODIS data in coastal (Huot et al., 2005) and ocean waters (Behrenfeld et al., 2009). However, although FLH was first applied to MODIS-Terra, this sensor has significantly degraded since its launch, resulting to low data quality (Blondeau-Patissier et al., 2014; Franz, 2008). Therefore, we refer primarily to the MODIS-Aqua sensor when we refer to MODIS. Although FLH based SIF retrievals dominated research, ample evidence indicate limitations of the FLH method in combination with MODIS and MERIS (Gilerson and Huot, 2017; Gons et al., 2008). The main drawback of SIF retrievals using FLH and data from above multispectral satellite is incapability to account for the shifting peak position with increasing backscattering (for limitations of FLH, see Section 4.1.). As consequence, a development of alternative methods was initialized (Gilerson et al.,

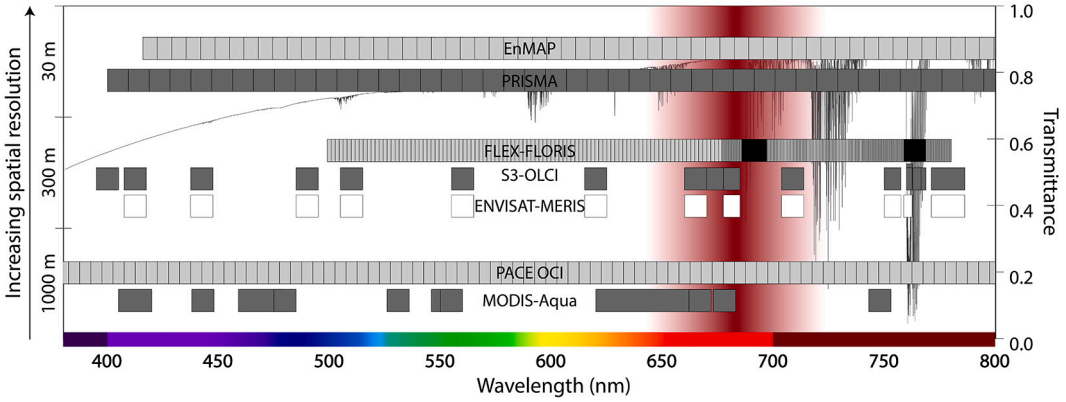

Fig. 2. Comparison of sensor specifications of satellites between 400-800 nm. Rectangular shapes signify sensor FWHM and spectral interval arranged from bottom to top according to increasing spatial resolution. White, dark grey and light grey indicate historical, current and future sensors, respectively. Atmospheric transmittance spectrum is included in the background (from MODTRAN simulation (Berk et al., 2005)). Red gradient in the red-NIR spectral region indicate SIF emission occurrence with darker shade indicating proximity to emission peak.

2008; Huot et al., 2007; Ioannou et al., 2009).

The Medium Resolution Spectral Imager II (MERSI II) onboard Feng Yun 3D satellite has been operational since 2017 (Xu et al., 2018). The specifications are similar to MERIS but there has not been studies published which retrieve SIF using MERSI II data. However, some studies have already been published using this sensor to monitor oceans and lakes (Chen et al., 2020, 2021).

Recently, atmospheric satellite sensors offering high spectral (~0.25–0.55 nm) but low spatial (7 km - 40 km) resolution were exploited for aquatic SIF studies (i.e. SCIAMACHY, GOME-2 and TROPOMI). Although designed for atmospheric research, the very narrow spectral bands and high SNR facilitate global SIF retrievals in ocean waters (Joiner et al., 2016; Köhler et al., 2020; Wolanin et al., 2015). Despite this success, the spatial resolution of such instruments is about an order of magnitude lower than suggested for optically complex waters (IOCCG, 2012).

The Hyperspectral Imager for the Coastal Ocean (HICO), temporarily installed onboard the International Space Station (ISS), is the first spectrometer dedicated to measure coastal ocean regions from space (Keith et al., 2014). A study by Ryan et al. (2014) successfully demonstrated SIF retrieval from HICO-data using the FLH approach to study phytoplankton dynamics in Monterey Bay. Dierssen et al. (2015) used the same data and approach to map the distribution and abundance of a ciliate bloom using phycoerythrin SIF in Long Island coasts.

There are several other operating sensors in space that may satisfy the resolution requirements for SIF retrieval but no results in the context of SIF have been published so far (appendix - Table A3). Such sensors include Hyperion, while resulting data have been successfully used to estimate water constituent in optically complex waters (Giardino et al., 2007) and detect surface scum (Kutser, 2009). GOCI data were used to assess phytoplankton dynamics (Lee et al., 2012). Furthermore, the DLR's (German Aerospace Center) Earth Sensing Imaging Spectrometer (DESIS) sensor (Alonso et al., 2019) and Italian Space Agency (ASIs) Precursor of the Application Mission (PRISMA) (Loizzo et al., 2016) were just launched recently. There are no publications yet on SIF studies using DESIS and PRISMA but their spectral resolution and range indicate potential for SIF-related applications (Table A3).

Various other spectrometer systems are in preparation and will provide new avenues for aquatic research in general and SIF retrieval in particular. The upcoming Plankton, Aerosol, Cloud, ocean Ecosystem (PACE) mission from NASA will carry the Ocean Color Instrument (OCI) and will be launched in 2022. Specifications of OCI such as temporal frequency, spectral resolution and range, and SNR are optimized for ocean color RS (Werdell et al., 2019). OCI is also designed to have no or minimal striping through its single-science-pixel rotating scanner (Werdell et al., 2019). Its spatial resolution of 1000 m is however suboptimal for coastal and inland water RS. The 2021 scheduled launch of Environmental Mapping and Analysis (EnMAP) from DLR will be carrying the Hyperspectral Imager (HSI) payload. The HSI was designed to fill the gap in space-based imaging spectroscopy for applications in terrestrial and aquatic systems (Guanter et al., 2015). EnMAP has a high spatial resolution of 30 m, an advantage for inland and coastal waters, but its spectral resolution of 8.1 nm might limit SIF applications and requires further evaluation. Finally, European Space Agency's (ESA) FLEX mission, the first satellite based imaging spectrometer dedicated to SIF measurements, will be launched in 2023. While FLEX was developed with a specific focus on terrestrial vegetation, its objectives and specifications are also relevant for aquatic SIF. FLEX aims to understand the seasonal variability in photosynthetic functioning and efficiency of vegetation in a global context (Drusch et al., 2017). FLEX will cover terrestrial regions including inland waters and coastal areas $\leq$50 km from the coastlines at 300 m spatial resolution. The most distinguishing aspect of FLEX is the spectral resolution and range of its two modules (FLORIS -LR, -HR). One module will have very high spectral resolution ranging from 0.1 to 0.5 nm in the oxygen bands (HR). The second module has relatively lower spectral resolution of 2 to 3 nm and spans from 500 to 740 nm (LR). FLEX will be flying in tandem with Sentinel-3, which carries OLCI and SLSTR. OLCI on its own already provides data suitable for ocean color purposes and combined with FLORIS will expand its applications in optically complex waters. OLCI's and SLSTR's coverage from VIS to SWIR provides opportunity to retrieve in-water constituent concentrations and IOPs. Aside from water quality indicators, the Sentinel-3 instruments will also provide additional support for FLORIS image processing such as data for atmospheric and geolocation corrections (Mohammed et al., 2019). Although, there are many positive attributes of the upcoming FLEX mission to SIF research in optically complex waters, its repeat cycle and SNR are some of its disadvantages. A comparison of selected historical, current and future satellite sensors are presented in Figure 2.

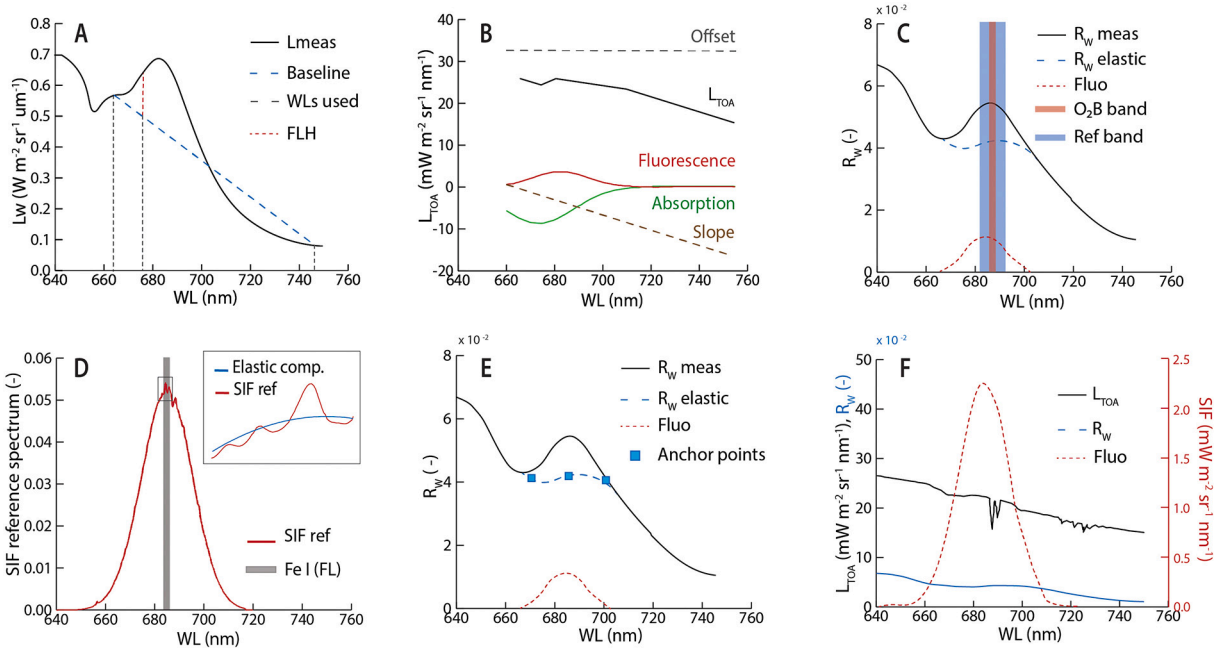

Fig. 3. Simple schematic of reviewed methods. A) FLH modified from Gilerson et al. (2007), B) OLCI Fluorescence Processor modified from Kritten et al. (2020), C) O_2B band differential absorption modified from Frouin et al. (2008), D) DOAS modified from Wolanin et al. (2015), E) ML regression modified from Tenjo et al. (2021), F) Spectral fitting modified from Meroni et al. (2010). Labels are described in the succeeding subsections.

4. Review of SIF retrieval methods

SIF retrieval schemes are required to compensate various effects impacting the measured radiance (cf. section 3) and to disentangle the reflected and emitted radiance contributions to this signal (cf. section 2). This section explores different retrieval techniques and their applicability to data acquired by the abovementioned sensors. A summary of relevant methods and their characteristics is given in the appendix (Table A4), the working principle of the individual methods is shown in Fig. 3.

All methods depend on a reliable accounting for atmospheric absorption and scattering effects to retrieve SIF either from L_{TOA} or water reflectance (R_W) data. The atmospheric compensation is one of the main challenges in characterizing water quality from spaceborne measurement. Several methods inherently compensate for atmospheric disturbances, while others do not and rely on properly corrected input data or availability of related atmospheric functions.

4.1. Fluorescence line height

The FLH method was developed by Gower (1980) and is still frequently used today. This simple algorithm uses three bands in the red to near infrared (NIR). The outer bands comprise two wavelengths not affected by SIF emissions. Both measurements serve the calculation of a virtual baseline by linear interpolation (Letelier and Abbott, 1996). The baseline represents backscattering and is subtracted from the center band to facilitate estimates of SIF. The used central band is located near the peak emission (≈685 nm) but outside the oxygen-B band (O_2B) at 687 nm to avoid perturbations by this strong absorption feature (Fig. 3). FLH based SIF retrieval is can be finally expressed as:

$$SIF_{FLH} = L_2 - [L_3 + (L_1 - L_3)(\lambda_3 - \lambda_2)/(\lambda_3 - \lambda_1)] \quad (4)$$

where λ corresponds to wavelength and subscripts refer to the three bands used. L in this case may refer to measured radiance (L_{meas}) in the form of water leaving radiance (L_W) or TOA radiance (L_{TOA}). L can also be substituted by R_W of RS reflectance (R_{rs}). FLH for MODIS uses three bands centered at 665, 678 and 746 nm, while FLH for MERIS utilizes bands at 665, 681 and 709 nm. Letelier and Abbott (1996) recommended normalizing FLH derived SIF values ($nSIF_{FLH}$) to correct for scattering, absorption and sensor geometry with respect to solar zenith angles.

FLH is easy to apply and several studies suggest retrieved SIF estimates as reliable proxy for [chl *a*], especially in areas where the blue-green band ratio algorithms fail (e.g. Gilerson and Huot, 2017; Gilerson et al., 2007; Gower, 2014). But the assumption of a straight baseline to represent elastic radiance is only valid when [chl *a*] is <10 mg m^{-3} (Gower et al., 2004). In cases where [chl *a*] and backscattering are high, the assumption of a linear baseline is violated and, therefore, affects the accuracy of retrieved SIF. While FLH was still effectively applied in some studies of optically complex waters (e.g. Gower and King, 2012; Palmer et al., 2015), other studies indicate that resulting SIF retrievals are only reasonable when [chl *a*] is 5–7 mg m^{-3} (Gilerson and Huot, 2017; Huot and Babin, 2010). Negative FLH values are observed when there is a reflectance peak shift from red to NIR (Palmer et al., 2015).

4.2. OLCI fluorescence peak height

The OLCI fluorescence peak height processor (FPH; Kritten et al., 2020) assumes that L_{TOA} can be represented with four components (cf. Fig. 3) and expressed as:

$$L_{TOA}(\lambda) = O + S\lambda + A\, e^{\left(\frac{(\lambda-\lambda_A)^2}{W_A}\right)} + SIF\, e^{\left(\frac{(\lambda-\lambda_F)^2}{W_F}\right)} \quad (5)$$

where O is offset and S is slope. A and SIF are amplitudes of Gaussian functions describing absorption and SIF wherein λ_A and λ_F are the center wavelengths of peak absorption and emission, respectively. $W_A = 18\ nm$ and $W_F = 15\ nm$ are the standard deviation of a gaussian based on FWHM of absorption and SIF emission bands, respectively. The equation was derived from extensive modelling experiments with the radiative transfer modelling scheme Matrix Operator Model (MOMO). It was found that L_{TOA} can be reliably approximated as function of the four components, while O and S accounts for atmospheric scattering and absorption contributions to L_{TOA} (Kritten et al., 2020). The retrieval of SIF is eventually based on model inversion.

The FPH can be used without explicit atmospheric correction since it inherently includes an approximation of atmospheric perturbances. The algorithm was found to provide reliable SIF estimates in waters with [chl a] ≥ 1 mg m^{-3} and was validated in regions with optically complex waters. However, the correlation between retrieved SIF and in-situ [chl a] suggests that improvement is needed to analyze water with [chl a] $<$ 1 mg m^{-3}. An offset between SIF and [chl a] was reported and associated to the simplified atmospheric compensation, particularly a missing correction of water vapor. The FPH can be also used with RS reflectance data where an improved correlation and a reduced offset between SIF and [chl a] was found (Kritten et al., 2020).

4.3. O_2B band differential absorption

Frouin et al. (2008) suggest a SIF retrieval approach targeting the O_2B absorption band to exploit the partial infilling of inelastic SIF (Fig. 3). SIF is conceptually expressed as difference between radiance in spectral bands with a higher relative contribution of SIF inside the absorption band (subscript 1) and in a spectral band less influenced by SIF outside of the absorption band (subscript 2). The method was developed for measurements just above the water surface and from space, while for the latter case SIF at the O_2-B band (683 nm) can be expressed as:

$$SIF_1 = \frac{L_{TOA,1} - L_{TOA,2}\, T_{O_2,1}(\theta_S, \theta_V, P_0)}{T_d(\theta_V)\left[h_1\, T_{O_2,1}(\theta_V, P_0) - h_2\, T_{O_2,1}(\theta_S, \theta_V, P_0)\right]} \tag{6}$$

where $T_{O_2,\ 1}(\theta_S, \theta_V, P_0)$ is the oxygen transmittance associated with elastic water reflectance and path radiance, θ_S is solar zenith angle, P_0 is pressure, θ_V is viewing zenith angle, T_d is diffuse atmospheric transmittance, h is a spectral function representing Gaussian distribution of fluorescence, and (θ_V,P_0) is the oxygen transmittance associated with SIF.

The working principle of this approach was demonstrated using synthetic data obtained from the Global Atmospheric Model (GAME) radiative transfer program and High Resolution Transmission (HITRAN) molecular spectroscopic database. Related sensitivity analysis by Frouin et al. (2008) indicate that using spectral bands centered over the O_2-B band (i.e. 683.1–692.0) provide more reliable SIF estimates compared to the use of a reference band next to the O_2B band (i.e. 681.0–686.0), mainly due to a stronger influence of elastic reflectance in the latter. Their simulations show that the method is applicable for both clear and optically complex waters, while significantly better accuracy can be achieved if the sensor is as close as possible to the water surface. This clearly indicates the severe impact of atmospheric effects when applied to TOA, particularly the vertical structure of aerosols. Their results still showed better accuracy compared to FLH but as of writing, there are no publications which apply this technique to measured data. The attenuation of SIF by oxygen requires modelling of the radiative transfer inside the oxygen band with a level of accuracy that presently has only been achieved with simulations. Using the Frouin et al. (2008) approach requires information on atmospheric conditions to properly account for varying oxygen concentration and diffuse atmospheric transmittance especially when applied to spaceborne measurements.

4.4. Differential optical absorption spectroscopy

Another SIF retrieval technique based on the exploitation of absorption features (i.e. Fraunhofer line Fe I at 684.3 nm) was developed by Wolanin et al. (2015). The adopted Differential Optical Absorption Spectroscopy (DOAS) approach exploits high and low frequency spectral features in the wavelength region of interest. Using a wavelength window spanning between 681.8 and 685.5 nm, the DOAS technique calculates molecular absorbers along the optical light path while elastic scattering is removed through fitting a low-degree polynomial (Fig. 3). A least squares minimization equation is used for fitting:

$$\left\| - ln(L(\lambda)/E_0(\lambda)\,) - \sigma_W(\lambda)S_W - SIF(\lambda)S_e - \sum_{k=0}^{K} a_k\lambda^k \right\|^2 \rightarrow min \tag{7}$$

where $L(\lambda)$ is backscattered radiance, $E_0(\lambda)$ is extraterrestrial irradiance, $\sigma_W(\lambda)S_W$ is water vapor reference spectrum multiplied to its scaling parameter, $SIF(\lambda)S_e$ is the SIF reference spectrum multiplied to its effective scaling parameter and $\sum_{k=0}^{K} a_k\lambda^k$ is the low order polynomial to remove broad band effects. $L(\lambda)$ and $E_0(\lambda)$ simulations were obtained using SCIATRAN, a coupled ocean-atmosphere radiative transfer model. Derivation of all parameters are detailed in Wolanin et al. (2015). This DOAS method was developed for use in open ocean waters, therefore effects of water vapor absorption and Raman scattering were included in the minimization. For optically complex waters, effects from water vapor and Raman scattering may be excluded.

This alternative method of retrieving fluorescence was used together with SCIAMACHY and GOME-2 data, wherein retrieved SIF of both approaches showed reasonable agreement with MODIS $nSIF_{FLH}$. The Wolanin et al. (2015) paper was the first demonstration of using hyperspectral satellite data to retrieve oceanic SIF. There is potential in applying the DOAS method to other water types although assumptions in the low order polynomial calculation to extract scattering effects must be cautiously reviewed to ensure all significant contributors to scattering and absorption are considered.

4.5. Machine learning regression

Another method to disentangle SIF from reflectance was developed by Tenjo et al. (2021) and expresses SIF as:

$$SIF(\lambda) = E_d(\lambda)\left[\rho_{app}(\lambda) - \rho_{real}(\lambda)\right] \tag{8}$$

where E_d is downwelling irradiance, ρ_{app} is apparent reflectance including SIF and ρ_{real} is real reflectance excluding SIF. E_d and ρ_{app} are obtained from atmospheric correction while ρ_{real} is estimated by interpolating the real reflectance within the SIF emission region through machine learning regression techniques and polynomial fitting methods. This method was developed by obtaining ρ_{real} using the Hydrolight radiative transfer model. A fraction of simulated ρ_{real} was used to train a machine learning (ML) algorithm and identify three anchor points within the wavelength region of ρ_{real} (i.e. 670, 685 and 700 nm). Considering validation results based on the remaining ρ_{real} simulations, an eight-degree polynomial derived by ML regression was found to optimally interpolate the three points and successfully estimate ρ_{real}.

4.6. Alternative retrieval approaches

Aside from all aforementioned methods, several past and recent studies suggest SIF retrieval techniques based on an inversion approach to be applied in coastal waters (e.g. Gilerson and Huot, 2017; Huot et al., 2007; Morrison, 2003) or in clear waters (Roesler and Perry, 1995). In general, this approach first performs an initial inversion of background radiance ≤650 nm to obtain IOPs. These IOPs are then used to simulate the elastic contribution to the wavelength region >650 nm by using a forward model. The difference between measured and modelled radiance is finally attributed to SIF (Morrison, 2003; Roesler and Perry, 1995). For the inversion, Levenberg-Marquardt optimization was the first choice by several authors (Gilerson and Huot, 2017; Huot et al., 2007; Roesler and Perry, 1995). Other used optimization methods were linear least squares fitting (Zhou et al., 2008) and non-linear least squares based on the Bates and Watts model (1998) (Morrison, 2003). Huot et al. (2007) suggests a Look-up table approach describing downwelling attenuation and backscattered radiance to provide the elastic component. Common to all these studies is that they have been mainly applied to in-situ measurements therefore, atmospheric absorption and scattering effects are not considered.

Yet other methods developed for terrestrial ecosystems might have potential for aquatic applications too, particularly the Spectral Fitting Method (SFM) and the Singular Value Decomposition (SVD) method. The SFM approach exploits the radiance signal acquired in high spectral resolution while focusing on the oxygen absorption bands O_2B and O_2A. The SFM approach assumes that a polynomial or another mathematical function can describe the spectral shape of reflectance and SIF (Meroni et al., 2010), while the at -sensor upwelling radiance is parametrized as:

$$L(\lambda) = \frac{r_{MOD}(\lambda)\, E(\lambda)}{\pi} + SIF_{MOD}(\lambda) + \varepsilon(\lambda) = L_{MOD}(\lambda) + SIF_{MOD}(\lambda) + \varepsilon(\lambda) \tag{9}$$

where $r_{MOD}(\lambda)$ and $SIF_{MOD}(\lambda)$ are functions describing the spectral shape of reflectance and SIF, respectively, $E(\lambda)$ is the incident solar irradiance, and $\varepsilon(\lambda)$ the modelling error. As expressed in Eq. 9, the SFM approach assumes a perfect atmospheric correction. The SIF retrieval relies on model inversion considering specific mathematical functions to describe the spectral shape of SIF and reflectance in the oxygen absorption wavelengths. Given a measured or simulated $E(\lambda)$ as model input, successive optimizations vary the reflectance and SIF shapes until the difference between the $L(\lambda)$ measured and simulated is minimized.

This approach, based on both modelling and spectral fitting, has already been validated for terrestrial vegetation at several acquisition scales. With appropriate modifications, it could be potentially suitable for other environments such as inland waters. In this framework, it is important to bear in mind that the radiation passes air and water, therefore correction factors between water-air interfaces are fundamental. Moreover, only SIF emitted in the visible red wavelength range is detectable due to water re-absorption. Finally, in optically complex waters, not only chl-*a* pigments emit SIF, but also other components affect the $L(\lambda)$ measured by the instruments, therefore the several variables in Eq. (9) need to be modelled adequately.

The SVD method was mostly used in retrieving SIF in the O_2A band region (~740 nm) in terrestrial ecosystems (e.g. Guanter et al., 2012; Köhler et al., 2015) but was recently applied for O_2B based SIF retrievals in oceanic waters using TROPOMI (Köhler et al., 2020). This data-driven method relies on a sub-nanometer resolution of satellite sensors to disentangle reflected radiance from SIF (Köhler et al., 2015). Modelling the low and high frequency contributors to reflected radiance enables estimates of SIF emission by evaluating changes in the fractional depth within the Fraunhofer lines. Köhler et al. (2020) executed this modelling approach using training data, i.e., spectra in non-fluorescent regions, and the SVD method to generate spectral functions (singular vectors) describing the non-SIF contributors to radiance. An optimization of a forward model including a summation of obtained singular vectors and a SIF contribution (represented by two spectral functions) enabled estimating SIF. This approach was found to be consistent with MODIS nFLH SIF estimates on a global scale (Köhler et al., 2020). It warrants further investigation in optically complex waters, especially when data from hyperspectral sensors with high spatial resolution become more widely available.

5. SIF applications

The availability of SIF estimates from multi-spectral sensor data such as MODIS and MERIS enabled various SIF applications for inland and coastal waters over the past two decades. The following sections focus on main satellite based applications: estimates of chl-*a*, detection of harmful algal blooms (HAB) and modelling of primary productivity (PP).

5.1. SIF based chl a estimates

SIF estimates have been historically used as linear approximation of [chl *a*], mainly in cases where other standard algorithms to retrieve [chl *a*] in the blue-green wavelength region fail. Several examples of this application are listed in the appendix (Table A5). A general finding of past studies is that reliable SIF based chl-*a* estimates are limited to a narrow range of chl *a* concentrations (i.e. [chl *a*] < 10 mg m^3) (e.g. Gilerson and Huot, 2017; Mckee et al., 2007) and reduced TSM concentrations (Gilerson et al., 2008).

Studies based on in-situ measurements report varying success in using SIF as proxy for [chl *a*] and the disturbing effect of water constituents on SIF chl *a* relationships. Gons et al. (2008), for example, report a good relationship between SIF and chl *a* ($r^2 = 0.8$) for oligotrophic conditions in the Great Lakes (appendix - Table A5), while the relationship became weak in regions with higher constituent concentrations. A wide range of chl *a* and TSM concentrations were considered in Nebraskan lakes (Gurlin et al., 2011), resulting in a low relationship ($r^2 = 0.22$). Gilerson et al. (2008) and Gilerson and Huot (2017) also found a systemic overestimation of SIF signal when NAP is >10 g m^{-3}, determining SIF as unreliable proxy for chl *a* when NAP concentrations change. Furthermore, Dall'Olmo and Gitelson (2005) demonstrated that chl *a* quantum yield of fluorescence and specific absorption coefficients affect remote sensing based estimates of [chl *a*].

Studies based on satellite data confirm above findings and partial limitations of SIF based chl *a* estimates. One example from Chesapeake Bay indicates that SIF from MODIS Level 2 (L2) data is well correlated with chl *a* concentrations up to 4–7 mg m^{-3} (Gilerson and Huot, 2017), but the relationship diminishes when NAP is larger than 5 g m^{-3}. A study focusing on coastal areas in Florida indicates a substantial improvement of SIF based chl *a* estimates compared to the use of blue-green chl *a* algorithms (Moreno-Madriñán and Fischer, 2013), but points to inaccuracies of SIF derived chl *a* due to stray light contamination and adjacency effects. Their study also contradicts other assessments since, showing that increasing turbidity does not affect FLH retrievals. Using MERIS Level 2 data, Gower and King (2007) found SIF to be a viable proxy for chl *a* concentrations up to 19 mg m^{-3} in western Canada coastal area. They also found that MERIS detects around 30% more SIF compared to MODIS due to the closer proximity of the MERIS band to the SIF emission peak.

5.2. SIF for algal bloom detection

SIF based monitoring of algal blooms in coastal (e.g. Hu et al., 2005; Lou and Hu, 2014; Wynne et al., 2008) and inland waters (Matthews et al., 2012) is mainly dependent on the relationship between SIF and chl *a*. Reported results are, thus, reliable for lower chl *a* concentrations (Hu et al., 2005; Matthews et al., 2012), while SIF was found to be less conclusive for bloom detection associated with very high chl *a* concentrations (Lou and Hu, 2014; Tomlinson et al., 2009). However, several studies report successful applications of SIF for HAB detection in specific environments or suggest SIF as future information source for sophisticated HAB approaches.

One example for a successful SIF application in this context is the detection of *K. brevis* blooms in coastal areas of Florida (Hu et al., 2005). *K. brevis* are dinoflagellates and produce toxins that cause water to look red or brown, a phenomenon commonly referred to as "red tides". These toxins can be accumulated by shellfish or kill marine animals and birds when ingested (Anderson, 2005). Since *K. brevis* have low backscattering due to their relatively large size, the signal obtained at ~680 nm is mainly attributed to SIF, while this assumption only holds for a chl *a* range between 0.4 and 4 mg m^{-3}. In contrast to the results by Hu et al. (2005), the study by Tomlinson et al. (2009) found the use of SIF to monitor *K. brevis* inconclusive. While they found that spatial patterns of SIF and chl *a* tend to coincide, there was an ambiguity of distinguishing whether the chl *a* anomalies stem from *K. brevis, Trichodesmium* spp. or other diatom species. Carvalho et al. (2011) also indicate the potential of SIF to infer *K. brevis* presence, but ranks SIF lower compared to other RS variables such as particulate backscattering and phytoplankton absorption. Applicability of SIF to monitor the diurnal cycle of *P. donghaiense* blooms was investigated in East China Sea (ECS) using GOCI data (Lou and Hu, 2014). *P. donghaiense* are non-toxic dinoflagellates typical in ECS but still harmful in coastal regions when biomass accumulates (Lu et al., 2005). ECS is characterized by high CDOM concentrations and, although theoretically sensitive, SIF was found to be ineffective in detecting *P. donghaiense* concentrations in such conditions in accordance with theory due to high absorption of $\dot{E}(PAR)$.

Several studies assessed HABs in their regions of interest using methods not requiring SIF but mentioned potential of including SIF in future work. For instance, the elevated quantum yield of SIF from diatoms (Nymark et al., 2009) can be exploited to distinguish between a diatom-dominated bloom from other phytoplankton types such as a dinoflagellate-dominated bloom in the Benguela System (Bernard et al., 2014). Another example is a study from Siswanto et al. (2013) where they developed a simple HAB detection processing chain for *K. mikimotoi* and diatom blooms in Seto Inland Sea using MODIS data. They used spectral shapes and empirical relationships to determine whether the water is TSM, CDOM or diatom dominated. Although the authors did not use SIF, they considered doing this in the future to lessen false positives due to CDOM.

5.3. SIF for quantum yield and primary productivity estimates

Aside from SIF, ϕ_F can also be retrieved to gain more information about phytoplankton physiology and consequently, primary productivity (P_C). According to (Kiefer et al., 1989), P_C can be expressed as:

$$P_C = \dot{E}(PAR)\,[chla]\,\bar{a}^*_\phi\,\phi_C \tag{12}$$

where P_C represents carbon assimilation in mol carbon m^{-3} s^{-1}, $\dot{E}(PAR)$ is scalar irradiance integrated from 400 nm to 700 nm, [*chl a*] is chl-*a* concentration, $\bar{a}^*_\phi$ is the irradiance-weighted chl-*a*-specific absorption coefficient of phytoplankton and ϕ_C is quantum yield of carbon fixation, equivalent to moles of carbon fixed for each mole of absorbed photon by cellular pigments. Including SIF quantities in Eq. (12), as shown by (Huot and Babin, 2010), results in:

$$P_C = \frac{4\pi\, SIF\,[K_{Lu}(\lambda_{em}) + K(PAR)]\,\phi_C}{Q_a\,\phi_F} \tag{13}$$

While $K(PAR)$ is the attenuation coefficient in the excitation irradiance, Q_a is the intracellular reabsorption of fluorescence, and $K_{Lu}(\lambda_{em})$ is the attenuation coefficient for upwelling radiance.

Key for productivity estimates is knowledge of all input parameters, while a particular focus in past literature is on ϕ_F and its relationship to photochemical processes. Past studies demonstrate the analytical (or semi-analytical) retrieval of ϕ_F for study areas spanning oligotrophic (Maritorena et al., 2000), mesotrophic (Morrison, 2003) and eutrophic waters (Zhou et al., 2008). Maritorena et al. (2000) derived ϕ_F using SIF estimates from in-situ upwelling and downwelling radiance measurements, in-situ [chl *a*] and in vitro absorption phytoplankton spectra. Morrison's (2003) method utilized inversion techniques to initially retrieve IOPs and use them later to correct for scattering contributions within the SIF emission band. Subsequently, calculated SIF and measured chl-*a* absorption were used to retrieve ϕ_F. Zhou et al. (2008) obtained ϕ_F in a similar manner as Morrison (2003) albeit with added complexity given the additional contribution of other in-water constituents. For the three studies, ϕ_F was measured during or near solar noon when downwelling irradiance is at its maximum. This led to low quantum yields of 1%, 0.84% and 0.33% for Maritorena et al. (2000), Morrison (2003) and Zhou et al. (2008), respectively. All studies indicated that ϕ_F may be attributed to NPQ mechanisms occurring at solar noon which lead to low SIF yields.

Although several authors have demonstrated how to retrieve ϕ_F, it is rare to find past studies which use satellite data to estimate ϕ_F in optically complex waters (e.g. Huot et al., 2005). This is due to challenges associated to the calculation of ϕ_F and the complexity to account for variable fluorescence and quenching mechanisms. Quantum yield of fluorescence already varies by ±10% without influence of non-algal particles (Mckee et al., 2007). The presence of CDOM and TSM can

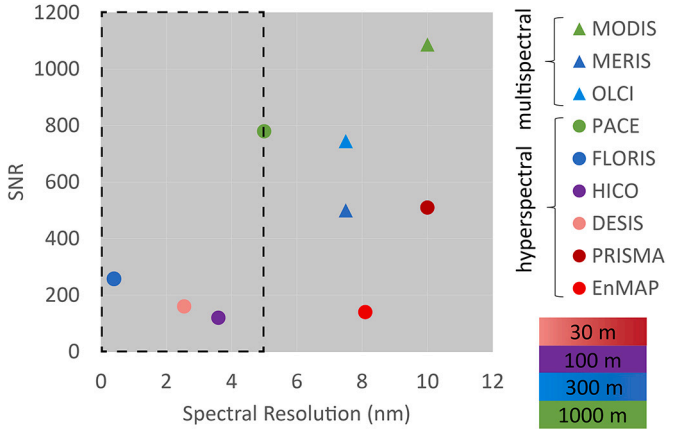

Fig. 4. Sensor characteristics of available and upcoming multi- and hyperspectral satellite missions. Shown characteristics include Signal-to-Noise-Ratio (SNR), spectral resolution at the SIF peak emission region (between 678–690 nm) and spatial resolution (color-coded). Points in the dashed box indicate sensors satisfying the spectral resolution threshold for fluorescence retrieval based on CEOS (2018).

also decrease or increase ϕ_F but differences due to changing constituent concentration is still within the range of the natural variability of ϕ_F (Mckee et al., 2007).

Biases associated with RS derived estimates of constituent concentrations and/or IOPs impact the success in deriving ϕ_F, and consequently *Pc*. For oceanic waters, Behrenfeld et al. (2009) developed a method which corrects for NPQ in ϕ_F estimates using averaged incident solar irradiance. They investigated phytoplankton physiology globally and found links between iron availability and ϕ_F, which provides insight how nutrient stress could affect aquatic ecosystems. Furthermore, Huot et al. (2013) developed an approach to minimize the aforementioned biases when calculating ϕ_F for the ocean but this approach could potentially be adopted for inland and coastal waters.

6. Synthesis and gap analysis

6.1. Observations

Several upcoming satellite missions are equipped with imaging spectrometers offering high spectral resolution (e.g. FLEX, EnMAP and PACE, with the latter specifically designed for aquatic ecosystems). The contiguous bands will facilitate advanced SIF retrieval methods to more reliably disentangle SIF from other radiance components compared to FLH. The high spectral resolution comes with a possibly lower SNR than required for aquatic applications. A plot showing the dependency of SNR and spectral resolution at the SIF emission peak wavelength region (i.e. 680 nm) is shown in Fig. 4. A general positive dependency is visible, i.e. lower spectral and spatial resolution corresponds to higher SNR and vice versa, but only four of the sensors (i.e. OCI, FLORIS, HICO and DESIS) satisfy the 5 nm spectral resolution necessary to characterize SIF emission in optically complex waters (CEOS, 2018). OCI and FLORIS are payloads of upcoming missions, DESIS is currently onboard ISS, while HICO was previously mounted in ISS and no longer active. OCI has the highest SNR of the four sensors but with lowest spatial (1000 m) and spectral (5 nm) resolution. Since OCI was designed for ocean water applications, its characteristics match ocean requirements better, but data may still be valid for larger inland and coastal water environments. FLORIS has the second highest SNR and highest spectral resolution (0.1–0.5 nm), since it was deliberately designed for SIF retrieval in terrestrial ecosystems. As largely demonstrated by MERIS and OLCI, its spatial resolution of 300 nm could facilitate assessments of optically complex waters with medium to larger sizes. HICO and DESIS both have spectral resolutions within the 5 nm threshold and, although their high spatial resolution would be an asset, their low SNR is a drawback which could limit aquatic applications.

Binning strategies spectrally and spatially can overcome some of the above limitations. FLORIS offers large margins for spectral binning to increase SNR while still maintaining the required threshold spectral resolution for SIF retrievals. For HICO and DESIS data, spatial binning (e.g. binning to 300 m) can also improve the SNR. Comparing the impact of binning to SNR while optimizing for spectral and spatial resolution should be assessed in the future.

The temporal resolution of satellite data is based on the coverage frequency of polar orbiting satellites (e.g. OCI and FLORIS) and the ISS orbit (i.e. DESIS and HICO). OCI and FLORIS have revisit periods of 16 and 27 days, respectively, DESIS and HICO provide irregular observations due to the varying orbit of the ISS. This frequency limits the application of satellite data to assess diurnal cycles in phytoplankton SIF emission. Although the combination of individual observations can shorten the sampling interval, only geostationary sensors would offer diel-sensing capability. However, Bracaglia et al. (2020) has shown that a virtual constellation of ocean color sensors could provide some capacity for hypertemporal assessments of sea-water optical properties. Besides GOCI and the GeoNEX constellation of geostationary satellites (i.e. GOES-16/17, Himawari-8/9, and several others) (Wang et al., 2020), offering hypertemporal and multispectral observations in 500 m pixel size for MODIS-like FLH retrieval, there is no current or planned geostationary sensor equipped with an imaging spectrometer dedicated for SIF observations. Therefore, the four above listed sensors will mainly facilitate assessments of seasonal and inter-annual dynamics besides other changes observable within the limits of the revisit periods.

6.2. Methods

SIF retrievals based on the FLH approach are only reliable for a narrow range of chl *a* and TSM concentrations due to the assumption of a linear elastic contribution within the SIF emission spectral region. Although the theoretical basis of phytoplankton SIF retrievals has been present for several decades, applying more advanced retrieval approaches has been so far limited by the availability of sensor data. The availability of more advanced observational technology facilitates but also asks for progress in method development and validation. In fact, several sophisticated methods to disentangle SIF from other radiance components are available in literature (cf. Section 4). A successful application of these methods for SIF retrieval in ocean and coastal waters have been demonstrated, but so far mainly with simulated data and only few observations from ocean color sensors (i.e. SCIAMACHY and Sentinel-3 OLCI). Intense developments and validation attempts are now needed to adapt and investigate the applicability of advanced SIF retrieval approaches for inland waters. These assessments should go beyond the use of simulated data and must include real observations, while more opportunities for method evaluation will arise with the increasing availability of new sensor data. A focal point of these assessments should be on advantages and disadvantages of new retrieval techniques by studying the range of water types where they work and whether this significantly expands the range of water types facilitated by the current FLH method. Further, uncertainties associated with physiological phytoplankton dynamics due to quenching mechanisms and how this affects SIF retrievals must be studied as well. Another important consideration in SIF retrieval is the atmospheric correction. One of the strengths of the FLH method is the implicit inclusion of the atmospheric correction and the simplicity of the method since L_{TOA} quantities may be used. However, most of the advanced SIF retrieval approaches require an explicit atmospheric correction. Determining a suitable atmospheric correction procedure for SIF retrieval methods depends largely on which wavelength regions are necessary to estimate SIF and interpret its dynamics. Particularly retrievals based on exploiting atmospheric oxygen features require precise estimates of the current atmospheric state. Further, the impact of sun glint and adjacency effects on SIF retrievals requires further investigation.

6.3. Applications

A main driver of technological and methodological development are applications, including [chl *a*] estimates, HAB detection and PP estimates. Past studies demonstrated the limited applicability of SIF as a proxy for [chl *a*] in lakes and coastal areas. The limitation is mainly attributed to disturbing effects of several water constituents on SIF-chl-*a* relationships as occurring in a wide range of water types (i.e. water with high TSM, high or low chl *a*) or due to adjacency effects. Generally, SIF

chl-*a* relationships diminish for chl *a* concentrations larger than 5 mg m^{-3} in most of the regions investigated and for too low chl *a* concentrations. Further, several assessments using field and satellite data found that elevated CDOM concentration contributes to challenges associated with the use of SIF for chl *a* estimates and highlight the significant effect of TSM concentrations larger than 5 g m^{-3} to weaken the relationships between chl *a* and SIF. The limited applicability of SIF as proxy for chl *a* mainly lies in the inefficiency of currently available methods to reliably disentangle SIF from other radiance components, particularly under high constituent concentrations. Further, low SIF emissions due to low chl *a* concentrations can be below the detection limit of the sensor and retrieval method. More robust SIF retrieval methods in combination with spectral high resolution data can be a way out to account for the disturbing effect of high water constituent concentrations when retrieving SIF. Whether the combination of sophisticated retrieval schemes and hyperspectral data considerably improve the range of water types where SIF estimates are successfully should be assessed in the near future.

For algal bloom detection, other algorithms (i.e. maximum peak height, cyanobacteria index) outperformed the use of SIF. In cases where SIF was successfully applied, the chl *a* concentration was in a specific range with relatively low values (i.e. chl $a < 4$ mg m^{-3} for *K. brevis* in Florida coasts or chl $a < 20$ mg m^{-3} in a South African bay). There is also an issue of ambiguity since SIF emission quantified with the FLH approach does not allow to directly differentiate taxa. First assessments suggest coupling SIF with other characteristics of phytoplankton (e.g. size distribution) to indicate which species are present. Also the combination of constituent retrievals with SIF (e.g. low SIF emissions at 680 nm together with high chl *a*) can be indicative to detect cyanobacteria (Simis and Huot, 2012). Hu et al. (2005) emphasized the need to combine SIF retrieved with other algal bloom indicators, i.e. phenology pattern of phytoplankton assemblages, and local knowledge of waters to aid with ambiguous SIF retrievals. Advanced HAB detection would require combined approaches to lessen monitoring uncertainties. In the future, diversity of SIF emission signals (IOCCG, 2014; Millie et al., 2002) due to varying pigments coupled with absorption features can aid in fine-tuning and distinguishing dominant species during a bloom event provided that methods and hyperspectral sensors provide sufficient information to resolve related spectral features.

ϕ_F as relevant indicator of phytoplankton physiology and productivity, can be estimated from SIF. However, ϕ_F is often estimated prior to SIF in optically complex waters rather than the other way around. Some efforts have been directed to develop ways to directly estimate ϕ_F in oceanic waters. Underlying assumptions, however, prevent applicability for most coastal or lacustrine areas (Behrenfeld et al., 2009; Huot et al., 2013). Studies deriving ϕ_F from satellite products for optically complex waters (Huot et al., 2005) are rare due to the need for several a priori information to derive ϕ_F including constituent concentrations and IOPs, both inherently contain biases that propagate when combined. More work is required to investigate uncertainty propagation of such retrievals to determine whether estimated ϕ_F would still be significant. Availability of variable fluorescence data from fluorometers should be exploited and investigated to derive meaningful relationships with SIF and ϕ_F.

Finally, light attenuation plays a significant role in the depth observable through RS techniques. Like with other ocean color applications, SIF based applications are often constrained to the uppermost layers of the water (Blondeau-Patissier et al., 2014). Although emitted SIF can sometimes be strong even at a deeper layer, strong attenuation of the upwelling radiance can significantly lessen detectability of the signal. Such conditions, therefore, impact SIF applications associated with retrieved SIF as well. Attenuation is also higher in the red-NIR than in green-blue wavelength region which entails shallower depth considered by SIF algorithms compared to ocean color algorithms (Wang et al., 2009). A possible workaround in conditions where the signal is higher than noise-equivalent water-leaving radiance would be to couple in-situ SIF obtained from vertical profilers with above water measurements. This would give us an understanding not only of the differences between SIF at various depths and above water SIF but also of where quenching mechanisms occur.

7. Conclusion

RS of phytoplankton SIF in coastal and inland waters can provide insights to trophic status, algal bloom development, and phytoplankton physiology. Studies from past decades enhanced our understanding on the dynamics of phytoplankton SIF and demonstrated the possible use of SIF as an optical indicator of ecological status in aquatic environments. We suggest taking advantage of emerging sensor technology offering high spectral resolution to provide unambiguous retrievals of SIF and SIF spectral diversity in relation to phytoplankton taxa and physiological state. We propose to invest in the development of new SIF retrieval schemes that are optimized for the rich information content provided by new sensor data. These new retrieval schemes should comprise strategies to compensate for possible sensor effects (e.g. low SNR, spectral non-uniformities, etc.) and atmospheric disturbances, and enable the exploitation of the full spectral signal to assess SIF and other information (e.g. light availability, quenching) required for specific applications. We conclude on the emerging increase of possible SIF applications and suggest developing process understating and mechanistic models in parallel to sensor and methodological advance. This ensures a qualified use of newest data for throughout assessments of dynamic processes in inland and coastal waters.

Declaration of Competing Interest

The authors declare that they have no known competing financial interests or personal relationships that could have appeared to influence the work reported in this paper.

Acknowledgments

The authors are grateful for the additional information provided by Michael Francois of ESA, Jeremy Werdell and Gerhard Meister of NASA, Carolina Tenjo and Luis Guanter of University of Valencia, Wesley Moses of the Naval Research Laboratory, Mariano Bresciani of CNR-IREA and Roberto Colombo and Sergio Cogliati of University of Milano Bicocca. The authors also appreciate the valuable comments and suggestions from the three anonymous reviewers which helped improve this study.

Appendix A

Table A1

Examples of field sensor specifications. This is a non-exhaustive list to demonstrate some commonly used sensors based on literature included in this review. Unshaded = sensors used in aquatic SIF research; Light grey = sensors not yet used specifically in aquatic SIF research.

Instrument	Under or above water measurement	FOV (^{0})	Spectral range (nm)	No. of spectral bands	Spectral sampling interval (nm)	FWHM (nm)	Reference
LI-1800	Underwater	3	305 - 800	~99	5	8	Maritorena et al., 2000
PNF 300	Underwater	26	665 - 740	1	NA	50	
PRR 600	Underwater	--	412 - 683	7	NA	10	Morrison, 2003
TSRB (now HyperTSRB)	Underwater	3	400 - 800	~123	3.3	3.3	Chetty et al., 2013
GER 1500	Under/Above water	3	350 - 1500	~766	1.5	3.2	Zhou et al., 2008
PR 650 Spectra-Colorimeter	Above water	7	380 - 780	~114	3.5	8	Gons et al., 2008
HyperOCR --	Underwater	8	350 - 800	~136	3.3	10	Vabson et al., 2019
HyperOCR ++	Above water	3	320 - 1050	~136	3.3	10	
RAMSES	Under/Above water	7	320 - 1050	~221	3.3	10	
WISP-3	Above water	3	380 - 800	~1700	0.4	3	
SeaPRISM	Above water	1.2	412 - 1020	8	NA	10	
SeaPRISM for Ocean Colour	Above water	1.2	412 - 1020	12	NA	10	
SeaPRISM for Lake Colour	Above water	1.2	412 - 1020	12	NA	10	
SR-3500	Above water	5	350 - 2500	~2150	1	3-8	
FLOXBox High res optic	Above water	25	650 - 800	~880	0.17	0.3	Cogliati et al., 2019
FLOXBox Low res optic	Above water	25	400 - 950	~845	0.65	1.5	

Table A2
Examples of airborne sensor specifications. This is a non-exhaustive list to demonstrate some commonly used sensors based on literature included in this review. Unshaded = sensors used in aquatic SIF research; Light grey = sensors not yet used specifically in aquatic SIF research.

Instrument	FOV (degrees)	Spectral range (nm)	No. of spectral bands	Spectral sampling interval (nm)	FWHM (nm)	Reference
FLI	14	430 - 805	up to ~285	1.3	2.6	Hollinger et al., 1987
CASI	--	403 - 946	up to ~330	1.6	2.6	Gower et al., 1999
PRISM	30.7	350 - 1050	250	2.8	3.5	Erickson et al., 2019
APEX	28	400 - 2500	up to 532	0.45 – 7.5	0.86 - 12.3	Schaepman et al., 2015
AVIRIS-NG	36	380 - 2510	425	5	5	Thorpe et al., 2017
AISA	--	437 - 891	32	--	--	Koponen et al., 2002
MIVIS	71	431 - 12700	up to ~520	VIS: 20, >VIS: 8 - 64	VIS: 20, >VIS: 9 - 540	Giardino et al., 2015
Hyplant FLUO	32.3	670 - 780	1024	0.11	0.25	Rascher et al., 2015
Hyplant DUAL	32.3	380 - 2500	626	1.7 - 5.5	4 - 13.3	

Table A3
Summary of spaceborne sensor specifications. Unshaded = sensors used in aquatic SIF research; Light grey = sensors used in ocean color RS but not yet used specifically in aquatic SIF research; Dark grey = Upcoming satellite missions with specifications that can be used in retrieval of SIF in optically complex waters.

Mission	Sensor	Spatial resolution (m)	Repeat cycle (days)	Spectral range (nm)	No. of Spectral bands	FWHM (nm)	Reference
Envisat	MERIS	300	35	390-1040	15	3.75 - 15	Bezy et al., 2000
Terra and Aqua platform	MODIS	250, 500, 1000	16	400-14400	36	9 - 500	Barnes et al., 2002
Envisat	SCIAMACHY	3000 x 6000	35	240-2380	> 1000s	0.22 - 1.48	Noel et al., 1998
Earth Observing-1 (EO-1)	Hyperion	30	16	356-1058 852-2577	70 172	10	Folkman et al., 2001
ISS	HICO	100	63	400 - 745 746 - 900	124	10 20	Corson et al., 2008
GOCI	GOCI	500	8x / day	412 - 965	8	10-40	Faure et al., 2008
MetOp - A/B	GOME-2	4000	29	240-315	1024	0.24-0.29	Munro et al., 2016
				311-403	1024	0.26-0.28	
				401-600	1024	0.44-0.53	
				590-790	1024	0.44-0.53	
Sentinel-5P	TROPOMI	7000 x 3500	16	270-495	1200	0.55	Veefkind et al., 2012
				710-775	600	0.55	
				2305-2385	800	0.25	
Sentinel3-A/B	OLCI	300	27	400-1020	21	2.5 - 40	Donlon et al., 2012
	SLSTR	500 (VIS-SWIR), 1000 (IR)		555 - 10850	11	19 - 905	
PRISMA	PRISMA	30	29	400 - 1010	66 171	12 12	Loizzo et al., 2016

				920 - 2505			
ISS	DESIS	30	No repeat cycle	400 - 1000	235	2.55	Krutz et al., 2019
Feng Yun 3D	MERSI	250, 1000	6	470 - 12000	25	20 - 1000	Xu et al., 2018
EnMAP	HSI	30	27	420 – 1000 900 - 2450	230	4-20	Guanter et al., 2015
FLEX	FLORIS LR	300	27	500 - 600 600 - 677 697 - 740	93	3 3 2	Coppo et al., 2017
	FLORIS HR			677 - 686 686 - 697 740 - 755 755 - 759 759 - 769 769 - 780	288	0.7 0.3 0.7 0.7 0.3 0.7	
PACE	OCI UV - NIR	1000	16	340-890	110	5	Werdell et al., 2019
	OCI SWIR			940 1038 1250 1378 1615 2130 2260	7	45 75 30 15 75 50 50	

Table A4
Summary of SIF retrieval methods, characteristics and input requirements.

Method	Reference	Scale of design	L_{TOA} or R_W based?	tmospheric data required	Multispectral or hyperspectral	Spectral band/range	Retrieved SIF	Mathematical procedure	RTM used	A priori information
						Fluorescence				

(*continued on next page*)

Table A4 (*continued*)

Method	Reference	Scale of design	L_{TOA} or R_W based?	tmospheric data required	Multispectral or hyperspectral	Spectral band/range		Retrieved SIF	Mathematical procedure	RTM used	A priori information (spaceborne measurements)
						Fluorescence	Non-fluorescence				
							Non-fluorescence				(spaceborne measurements)
FLH	Gower (1990) and Letelier and Abbott (1996)	Field, Airborne, Satellite	L_{TOA}	None	Multispectral	667, 678, 746 (MODIS) 665, 681, 709 (MERIS)	667, 746 (MODIS) 665, 709 (MERIS)	Scalar	Arithmetic	None	1. LTOA
OLCI Fluorescence Processor	Kritten et al. (2020)	Field, Satellite	L_{TOA} or R_W	None (Lu), atmospheric correction (R_W)	Multispectral (extendable to hyperspectral)	665, 674, 681, 709, 754 (OLCI)	–	Spectrum	Numerical	MOMO	LTOA or R_W (Sentinel-3: OLCI)
O2B band differential absorption	Frouin et al. (2008)	Model simulations	R_W	O2B transmissivity, aerosol optical thickness	Hyperspectral	686.8–688.3	683.1–692	Spectrum	Numerical	GAME	1. R_W 2. Function characterizing SIF emission 3. Spectral domain 4. Oxygen and diffuse atmospheric transmittance
DOAS	Wolanin et al. (2015)	Model simulations, Satellite	R_W	ATMOSPHERIC correction	hyperspectral	681.8–681.5	370–720	Spectrum	Numerical	SCIATRAN	1. R_W 2. Function characterizing SIF emission 3. Modelled reference spectra for fluorescence and water vapor from SCIATRAN 4. Low degree polynomial to remove broadband effects 5. Scaling factors for reference spectra
ML regression	Tenjo et al. (2021)	Model simulations	R_W	Atmospheric correction	Hyperspectral	670–700	~640–750	Spectrum	Numerical	Hydrolight	1. R_W 2. Anchor points 3. Polynomial for interpolating anchor points
Spectral Fitting	Meroni et al. (2010) Cogliati et al. (2015)	Model simulations	L_{TOC} and R_W	Atmospheric correction	Hyperspectral	686.7–688.3	677–697	Spectrum	Numerical	FluorSAIL 3.0 (terrestrial SIF)	1. Top of canopy radiance 2. Downwelling radiance
Other inversion techniques	Roesler and Perry (1995)	Field	R_W	Atmospheric correction	hyperspectral	660–730	390–750	Spectrum	Numerical	RTE (Ronald & Zaneveld, 1982)	1. R_W 2. In-water constituent concentrations 3. IOPs 4. RTE
	Huot et al. (2007)	Field	R_W	Atmospheric correction	hyperspectral	650–700	380–700	Spectrum	Numerical	Hydrolight	1. R_W 2. Kd 3. RTM-based LUTs

Table A5 Overview of some applications where remotely sensed SIF was used in phytoplankton biomass and harmgul algal bloom investigations.

Application focus	Reference	Location	Data used	chl-*a* (mg m^{-3})	TSM (g m^{-3})	CDOM (m^{-1})	Z(SD) (m)	Satisfactory output?	Comments
1. Biomass and trophic status	Gons et al. (2008)	Lake Erie	Field data	0.37–131	–	0.11–1.9	0.4–15.8	Worked in oligotrophic conditions but failed in mesotrophic and eutrophic waters	
			MERIS	0.37–0-75	–	0.11–0.20	8.3–15.8	Failed in oligotrophic waters	
	Gurlin et al. (2011)	Fremont Lakes	Field data	2.27–200.81	1.19–15	0.46–1.45	0.51–4.20	Failed in oligotrophic waters	Poor correlation between chl-*a* and FLH
	Palmer et al. (2015a,b)	Lake Balaton	MERIS	1.5–57	2 to 70 (typical)	0.01–0.3	0.2–1.8 (typical)	Worked in conditions tested	Strong negative correlation between chl-*a* and FLH
	Gower and King (2007)	West coast of Canada	MERIS	~0.1–20	–	–	–	Worked in conditions tested	Correlation with FLH obtained using Algal 1 chl-*a* product
	Zhao and Cao (2012)	South China Sea	MODIS	0.065–1.74	–	~0.6	–	Worked in coastal area but failed in oligotrophic conditions	Failure attributed to MODIS detection limit and NPQ
	Salyuk et al. (2010)	Sea of Japan	MODIS	~0.1–6.5	–	–	–	Worked in areas with chl-*a* > 3	
	Gilerson et al. (2008)	Chesapeake Bay and Florida coast	MODIS and MERIS	9–354	7–64.8	0.55–5.6	–	Correlation works in chl-*a* < 4 (tested using simulated data) and TSM < 4	Failure mostly attributed to NAP concentration rather than quantum yield of fluorescence
	Gilerson and Huot (2017)	Chesapeake Bay and Nebsraka lakes	MODIS and MERIS	0.74–200	0.1–21.6	0.125–1.46	–	Worked for chl-*a* between 5 and 7 mg/ m3	Strong influence of high suspended matter concentration to FLH failure
	Mckee et al. (2007)	NA	MODIS simulations	0.1–10	0–10	0–1		FLH underestimates chl-*a* at low concentrations and fails when suspended matter is greater than 5	Strong influence of high suspended matter concentration to FLH failure
	Moreno-madriñán and Fischer (2013)	Tampa Bay	MODIS	4.18–11 (average)	0–70	–	0.1–8.8	Worked in stations >5 km from the shore	Attributed FLH performance to stray light and adjacency effects rather than turbidity
2. HAB detection	Hu et al. (2005)	Florida coast	MODIS	~0.4–5	–	–	–	Worked best in chl-*a* 0.4–4	Found to be effective in detecting *K. brevis* blooms
	Tomlinson et al. (2009)		SeaWiFS, MODIS	–	–	–	–	Inconclusive results	In-situ chl-*a* not mentioned, *K. brevis* cell count used in the study
	Carvalho et al. (2011)		MODIS	–	–	–	–	Ineffective	In-situ chl-*a* not mentioned, *K. brevis* cell count used in the study
	Matthews et al. (2012)	South African lakes and coast	MERIS	0.5–26.85	–	–	–	Worked in chl-*a* < 20	
	Wynne et al. (2013)	Lake Erie	MERIS	–	–	–	–	Unnecessary due to similarity with CI	Used chl-derived from MERIS and MODIS
	Lou and Hu (2014)	Zhejiang coast	GOCI	0.1–100	–	–	–	Ineffective due to increased backscattering signal	
	Gokaraju et al. (2011)	Gulf of Mexico	SeaWiFS, MODIS	–	–	–	–	Ineffective due to shallow waters	

References

Abbott, M.R., Letelier, R.M., 1996. Algorithm Theoretical Basis Document Chlorophyll Fluorescence (MODIS Product Number 20), pp. 1–42.

Alonso, K., Bachmann, M., Burch, K., Carmona, E., Cerra, D., de los Reyes, R., Dietrich, D., Heiden, U., Hölderlin, A., Ickes, J., Knodt, U., Krutz, D., Lester, H., Müller, R., Pagnutti, M., Reinartz, P., Richter, R., Ryan, R., Sebastian, I., Tegler, M., 2019. Data products, quality and validation of the DLR earth sensing imaging spectrometer (DESIS). Sensors (Switzerland) 19, 1–44. https://doi.org/10.3390/s19204471.

Anderson, D.M., 2005. The Ecology and Oceanography of Harmful Algal Blooms Multidisciplinary Approaches to Research by.

Babin, M., Morel, A., Gentili, B., 1996. Remote sensing of sea surface sun-induced chlorophyll fluorescence: consequences of natural variations in the optical characteristics of phytoplankton and the quantum yield of chlorophyll a fluorescence. Int. J. Remote Sens. 17, 2417–2448. https://doi.org/10.1080/01431169608948781.

Behrenfeld, M.J., Westberry, T.K., Boss, E.S., O'Malley, R.T., Siegel, D.A., Wiggert, J.D., Franz, B.A., McClain, C.R., Feldman, G.C., Doney, S.C., Moore, J.K., Dall'Olmo, G., Milligan, A.J., Lima, I., Mahowald, N., 2009. Satellite-detected fluorescence reveals

global physiology of ocean phytoplankton. Biogeosciences 6, 779–794. https://doi.org/10.5194/bg-6-779-2009.
Berk, A., Anderson, G.P., Acharya, P.K., Bernstein, L.S., Muratov, L., Lee, J., Fox, M., Adler-Golden, S.M., Chetwynd, J.H., Hoke, M.L., Lockwood, R.B., Gardner, J.A., Cooley, T.W., Borel, C.C., Lewis, P.E., 2005. MODTRAN5: A reformulated atmospheric band model with auxiliary species and practical multiple scattering options. Proceedings of the Society of Photo-Optical Instrumentation Engineer 5655, 662–667.
Bernard, S., Pitcher, G., Evers-king, H., Robertson, L., Matthews, M., Rabagliati, A., Balt, C., 2014. Remote sensing of the African seas. Remote Sens. African Seas 185–203. https://doi.org/10.1007/978-94-017-8008-7.
Bismarck, J. Von, Fischer, J., 2013. An examination of errors in computed water-leaving radiances due to a simplified treatment of water Raman scattering effects. AIP Conf. Proc. 1531, 939–942. https://doi.org/10.1063/1.4804926.
Bissett, P.W., Arnone, R.A., Davis, C.O., Dickey, T.D., Dye, D., Kohler, D.D.R., Gould, R. W., 2004. From meters to kilometers: a look at ocean-color scales of variability, spatial coherence, and the need for fine-scale remote sensing in coastal ocean optics. Oceanography 17, 32–43. https://doi.org/10.5670/oceanog.2004.45.
Blondeau-Patissier, D., Gower, J.F.R.R., Dekker, A.G., Phinn, S.R., Brando, V.E., 2014. A review of ocean color remote sensing methods and statistical techniques for the detection, mapping and analysis of phytoplankton blooms in coastal and open oceans. Prog. Oceanogr. 123, 123–144. https://doi.org/10.1016/j.pocean.2013.12.008.
Bracaglia, M., Santoleri, R., Volpe, G., Colella, S., Benincasa, M., Brando, V.E., 2020. A virtual geostationary ocean color sensor to analyze the coastal optical variability. Remote Sens. 12 https://doi.org/10.3390/rs12101539.
Carvalho, G.A., Minnett, P.J., Banzon, V.F., Baringer, W., Heil, C.A., 2011. Long-term evaluation of three satellite ocean color algorithms for identifying harmful algal blooms (Karenia brevis) along the west coast of Florida: a matchup assessment. Remote Sens. Environ. 115, 1–18. https://doi.org/10.1016/j.rse.2010.07.007.
CEOS, 2018. Feasibility Study for an Aquatic Ecosystem Earth Observing System, p. 195.
Chen, J., He, X., Liu, Z., Xu, N., Ma, L., Xing, Q., Hu, X., Pan, D., 2020. An approach to cross-calibrating multi-mission satellite data for the open ocean. Remote Sens. Environ. 246 https://doi.org/10.1016/j.rse.2020.111895.
Chen, S., Zheng, X., Li, X., Wei, W., Du, S., Guo, F., 2021. Vicarious radiometric calibration of ocean color bands for fy-3d/mersi-ii at Lake Qinghai, China. Sensors (Switzerland) 21, 1–18. https://doi.org/10.3390/s21010139.
Cogliati, S., Verhoef, W., Kraft, S., Sabater, N., Alonso, L., Vicent, J., Moreno, J., Drusch, M., Colombo, R., 2015. Retrieval of sun-induced fluorescence using advanced spectral fitting methods. Remote Sens. Environ. 169, 344–357. https://doi.org/10.1016/j.rse.2015.08.022.
Collins, D.J., Kiefer, D.A., Soohoo, J.B., Stuart McDermid, I., 1985. The role of reabsorption in the spectral distribution of phytoplankton fluorescence emission. Deep Sea res. Part A, Oceanogr. Res. Pap. 32, 983–1003. https://doi.org/10.1016/0198-0149(85)90040-8.
Dall'Olmo, G., Gitelson, A.A., 2005. Effect of bio-optical parameter variability and uncertainties in reflectance measurements on the remote estimation of chlorophyll-a concentration in turbid productive waters: modeling results. Appl. Opt. 45, 3577–3592. https://doi.org/10.1364/AO.45.003577.
Di Cicco, A., Gupana, R., Damm, A., Colella, S., Fiorani, L., Artuso, F., Brando, V.E., Lai, A., Genageli, A., Miglietta, F., Santoleri, R., 2020. "Flex 2018" Cruise: An Opportunity to Assess Phytoplankton Chlorophyll Fluorescence Retrieval at Different Observative Scales. Mediterranean Coastal Monitoring - CNR, Firenze, pp. 1–10.
Dierssen, H., McManus, G.B., Chlus, A., Qiu, D., Gao, B.C., Lin, S., 2015. Space station image captures a red tide ciliate bloom at high spectral and spatial resolution. Proc. Natl. Acad. Sci. U. S. A. 112, 14783–14787. https://doi.org/10.1073/pnas.1512538112.
Doerffer, R., 1993. Estimation of primary production by observation of solar-stimulated fluorescence. ICES Mar. Sci. Symp. 197, 104–113.
Drusch, M., Moreno, J., Bello, U. Del, Franco, R., Goulas, Y., Huth, A., Kraft, S., Middleton, E.M., Miglietta, F., Mohammed, G., Nedbal, L., Rascher, U., Schüttemeyer, D., Verhoef, W., 2017. Concept — ESA's earth explorer 8. IEEE Trans. Geosci. Remote Sens. 55, 1273–1284.
Erickson, Z.K., Frankenberg, C., Thompson, D.R., Thompson, A.F., Gierach, M., 2019. Remote sensing of chlorophyll fluorescence in the ocean using imaging spectrometry: toward a vertical profile of fluorescence. Geophys. Res. Lett. 46, 1571–1579. https://doi.org/10.1029/2018GL081273.
Falkowski, P., Kiefer, D.A., 1985. Chlorophyll a fluorescence in phytoplankton: relationship to photosynthesis and biomass. J. Plankton Res. 7, 715–731. https://doi.org/10.1093/plankt/7.5.715.
Franz, B.A., 2008. Moderate resolution imaging Spectroradiometer on Terra: limitations for ocean color applications. J. Appl. Remote. Sens. 2, 023525 https://doi.org/10.1117/1.2957964.
Frouin, R., Deschamps, P.-Y., Dubuisson, P., 2008. Remote sensing of solar-stimulated phytoplankton chlorophyll absorption in the oxygen B-band. In: Proc.SPIE 715005. https://doi.org/10.1117/12.806386.
Frouin, R.J., Franz, B.A., Ibrahim, A., Knobelspiesse, K., Ahmad, Z., Cairns, B., Chowdhary, J., Dierssen, H.M., Tan, J., Dubovik, O., Huang, X., Davis, A.B., Kalashnikova, O., Thompson, D.R., Remer, L.A., Boss, E., Coddington, O., Deschamps, P.Y., Gao, B.C., Gross, L., Hasekamp, O., Omar, A., Pelletier, B., Ramon, D., Steinmetz, F., Zhai, P.W., 2019. Atmospheric correction of Satellite Ocean-color imagery during the PACE era. Front. Earth Sci. 7, 1–43. https://doi.org/10.3389/feart.2019.00145.
Fujiki, T., Taguchi, S., 2002. Variability in chlorophyll a specific absorption coefficient in marine phytoplankton as a function of cell size and irradiance. J. Plankton Res. 24, 859–874. https://doi.org/10.1093/plankt/24.9.859.
Gege, P., Dekker, A.G., 2020. Spectral and radiometric measurement requirements for inland, coastal and reef waters. Remote Sens. 12 https://doi.org/10.3390/rs12142247.
Giardino, Claudia, Brando, Vittorio E., Dekker, Arnold G., Strömbeck, Niklas, Candiani, Gabriele, 2007. Assessment of water quality in Lake Garda (Italy) using Hyperion. Remote Sens. Environ. 109 (2), 183–195. https://doi.org/10.1016/j.rse.2006.12.017.
Giardino, C., Bresciani, M., Valentini, E., Gasperini, L., Bolpagni, R., Brando, V.E., 2015. Airborne hyperspectral data to assess suspended particulate matter and aquatic vegetation in a shallow and turbid lake. Remote Sens. Environ. 157, 48–57. https://doi.org/10.1016/j.rse.2014.04.034.
Gilerson, A., Huot, Y., 2017. Bio-optical modeling of Sun-induced chlorophyll- a fluorescence. In: Bio-Optical Modelling and Remote Sensing of Inland Waters. Elsevier Inc. https://doi.org/10.1016/B978-0-12-804644-9.00007-0
Gilerson, A., Zhou, J., Hlaing, S., Ioannou, I., Schalles, J., Gross, B., Moshary, F., Ahmed, S., 2007. Fluorescence component in the reflectance spectra from coastal waters. Dependence on water composition. Opt. Express 15, 15702–15721. https://doi.org/10.1364/OE.15.015702.
Gilerson, A.A., Zhou, J., Hlaing, S., Ioannou, I., Gross, B., Moshary, F., Ahmed, S.A., 2008. Fluorescence component in the reflectance spectra from coastal waters. II. Performance of retrieval algorithms. Opt. Express 16, 2446–2460. doi:https://doi.org/10.1364/OE.16.002446.
Gokaraju, B., Durbha, S.S., King, R.L., Younan, N.H., 2011. A machine learning based spatio-temporal data mining approach for detection of harmful algal blooms in the Gulf of Mexico. IEEE J. Sel. Top. Appl. Earth Obs. Remote Sens. 4 (3), 710–720. https://doi.org/10.1109/JSTARS.2010.2103927.
Gons, H.J., Auer, M.T., Effler, S.W., 2008. MERIS satellite chlorophyll mapping of oligotrophic and eutrophic waters in the Laurentian Great Lakes. Remote Sens. Environ. 112, 4098–4106. https://doi.org/10.1016/j.rse.2007.06.029.
Gordon, H.R., 1979. Diffuse reflectance of the ocean: the theory of its augmentation by chlorophyll a fluorescence at 685 nm. Appl. Opt. 18, 1161–1166. https://doi.org/10.1364/AO.18.001161.
Gower, J.F.R., 1980. Observations of *in situ* fluorescence of chlorophyll-*a* in Saanich Inlet. Boundary-Layer Meteorol. 18, 232–245. https://doi.org/10.1007/BF00122022.
Gower, J.F.R., 2014. A simpler picture of satellite chlorophyll fluorescence. Remote Sens. Lett. 5, 583–589. https://doi.org/10.1080/2150704X.2014.940630.
Gower, J.F.R., Borstad, G.A., 1990. Mapping of phytoplankton by solar-stimulated fluorescence using an imaging spectrometer. Int. J. Remote Sens. 11, 313–320. https://doi.org/10.1080/01431169008955022.
Gower, J.F.R., Borstad, G.A., 2004. On the potential of MODIS and MERIS for imaging chlorophyll fluorescence from space. Int. J. Remote Sens. 25, 1459–1464. https://doi.org/10.1080/01431160310001592445.
Gower, J., King, S., 2007. Validation of chlorophyll fluorescence derived from MERIS on the west coast of Canada. Int. J. Remote Sens. 28, 625–635. https://doi.org/10.1080/01431160600821010.
Gower, J., King, S., 2012. Use of satellite images of chlorophyll fluorescence to monitor the spring bloom in coastal waters, p. 1161. https://doi.org/10.1080/01431161.2012.685979.
Gower, James, Doerffer, R., Borstad, G., 1999. Interpretation of the 685nm peak in water-leaving radiance spectra in terms of fluorescence, absorption and scattering, and its observation by MERIS. Int. J. Remote Sens. 20, 1771–1786. https://doi.org/10.1080/014311699212470.
Gower, J.F.R., Brown, L., Borstad, G.A., 2004. Observation of chlorophyll fluorescence in west coast waters of Canada using the MODIS satellite sensor. Can. J. Remote. Sens. 30, 17–25. https://doi.org/10.5589/m03-048.
Graff, J.R., Behrenfeld, M.J., 2018. Photoacclimation responses in subarctic Atlantic phytoplankton following a natural mixing-restratification event. Front. Mar. Sci. 5, 1–11. https://doi.org/10.3389/fmars.2018.00209.
Groom, S.B., Sathyendranath, S., Ban, Y., Bernard, S., Brewin, B., Brotas, V., Brockmann, C., Chauhan, P., Choi, J.K., Chuprin, A., Ciavatta, S., Cipollini, P., Donlon, C., Franz, B.A., He, X., Hirata, T., Jackson, T., Kampel, M., Krasemann, H., Lavender, S.J., Pardo-Martinez, S., Melin, F., Platt, T., Santoleri, R., Skakala, J., Schaeffer, B., Smith, M., Steinmetz, F., Valente, A., Wang, M., 2019. Satellite Ocean colour: current status and future perspective. Front. Mar. Sci. 6 https://doi.org/10.3389/fmars.2019.00485.
Guanter, L., Frankenberg, C., Dudhia, A., Lewis, P.E., Gómez-Dans, J., Kuze, A., Suto, H., Grainger, R.G., 2012. Retrieval and global assessment of terrestrial chlorophyll fluorescence from GOSAT space measurements. Remote Sens. Environ. 121, 236–251. https://doi.org/10.1016/j.rse.2012.02.006.
Guanter, L., Kaufmann, H., Segl, K., Foerster, S., Rogass, C., Chabrillat, S., Kuester, T., Hollstein, A., Rossner, G., Chlebek, C., Straif, C., Fischer, S., Schrader, S., Storch, T., Heiden, U., Mueller, A., Bachmann, M., Mühle, H., Müller, R., Habermeyer, M., Ohndorf, A., Hill, J., Buddenbaum, H., Hostert, P., Van Der Linden, S., Leitão, P.J., Rabe, A., Doerffer, R., Krasemann, H., Xi, H., Mauser, W., Hank, T., Locherer, M., Rast, M., Staenz, K., Sang, B., 2015. The EnMAP spaceborne imaging spectroscopy mission for earth observation. Remote Sens. 7, 8830–8857. https://doi.org/10.3390/rs70708830.
Gurlin, D., Gitelson, A.A., Moses, W.J., 2011. Remote estimation of chl-a concentration in turbid productive waters — Return to a simple two-band NIR-red model? Remote Sens. Environ. 115 (12), 3479–3490. https://doi.org/10.1016/j.rse.2011.08.011.
Hu, C., Feng, L., 2016. Modified MODIS fluorescence line height data product to improve image interpretation for red tide monitoring in the eastern Gulf of Mexico. J. Appl. Remote. Sens. 11, 012003 https://doi.org/10.1117/1.jrs.11.012003.
Hu, C., Muller-Karger, F.E., Taylor, C., Carder, K.L., Kelble, C., Johns, E., Heil, C.A., 2005. Red tide detection and tracing using MODIS fluorescence data: a regional

example in SW Florida coastal waters. Remote Sens. Environ. 97, 311–321. https://doi.org/10.1016/j.rse.2005.05.013.
Hu, C., Feng, L., Lee, Z., Davis, C.O., Mannino, A., Mcclain, C.R., Franz, B.A., 2012. Dynamic range and sensitivity requirements of satellite ocean color sensors: learning from the past, p. 51.
Huot, Y., 2004. Sun-induced Fluorescence of Phytoplankton in the Ocean: Linking Physiology and Remote Sensing by Yannick Huot Submitted in Partial Fulfillment of the Requirements 1–359.
Huot, Y., Babin, M., 2010. Chlorophyll a Fluorescence in Aquatic Sciences. Methods and Applications. https://doi.org/10.1007/978-90-481-9268-7.
Huot, Y., Brown, C.A., Cullen, J.J., 2005. Oceanography: Methods New Algorithms for MODIS Sun-Induced Chlorophyll Fluorescence and a Comparison with Present Data Products 108–130.
Huot, Y., Brown, C.A., Cullen, J.J., 2007. Retrieval of phytoplankton biomass from simultaneous inversion of reflectance, the diffuse attenuation coefficient, and Sun-induced fluorescence in coastal waters. J. Geophys. Res. Ocean. 112, 1–26. https://doi.org/10.1029/2006JC003794.
Huot, Y., Franz, B.A., Fradette, M., 2013. Estimating variability in the quantum yield of Sun-induced chlorophyll fluorescence: a global analysis of oceanic waters. Remote Sens. Environ. 132, 238–253. https://doi.org/10.1016/j.rse.2013.01.003.
Ibrahim, A., Franz, B.A., Ahmad, Z., Bailey, S.W., 2019. Multiband atmospheric correction algorithm for ocean color retrievals. Front. Earth Sci. 7, 1–15. https://doi.org/10.3389/feart.2019.00116.
Ioannou, I., Zhou, J., Gilerson, A., Gross, B., Moshary, F., Ahmed, S., 2009. New algorithm for MODIS chlorophyll fluorescence height retrieval: performance and comparison with the current product. Remote Sens. Ocean 2009 (7473), 747309. https://doi.org/10.1117/12.830630.
IOCCG, 1998. Minimum Requirements for an Operational Ocean-Colour Sensor for the Open Ocean. Reports of the International Ocean Colour Coordinating Group. IOCCG, Dartmouth, Canada.
IOCCG, 2000. Reports of the International Ocean-Colour Coordinating Group Remote Sensing of Ocean Colour in Coastal, and Other Optically-Complex, Waters, Reports and Monographs of the International OceanColour Coordinating Group.
IOCCG, 2012. Mission Requirements for Future Ocean-Colour Sensors. Reports Ofthe International Ocean-Colour Coordinating Group. IOCCG, Dartmouth, Canada.
IOCCG (Ed.), 2014. Phytoplankton Functional Types from Space, no, 15th ed. IOCCG, Dartmouth, Canada.
Joiner, J., Yoshida, Y., Guanter, L., Middleton, E.M., 2016. New methods for the retrieval of chlorophyll red fluorescence from hyperspectral satellite instruments: simulations and application to GOME-2 and SCIAMACHY. Atmos. Meas. Tech. 9, 3939–3967. https://doi.org/10.5194/amt-9-3939-2016.
Keith, Darryl J., Schaeffer, Blake A., Lunetta, Ross S., Gould Jr., Richard W., Rocha, Kenneth, Cobb, Donald J., 2014. Remote sensing of selected water-quality indicators with the hyperspectral imager for the coastal ocean (HICO) sensor. Int. J. Remote Sens. 35 (9), 2927–2962. https://doi.org/10.1080/01431161.2014.894663.
Kiefer, D.A., Chamberlin, W.S., Booth, C.R., 1989. Natural fluorescence of chlorophyll a: relationship to photosynthesis and chlorophyll concentration in the western South Pacific gyre. Limnol. Oceanogr. 34, 868–881. https://doi.org/10.4319/lo.1989.34.5.0868.
Köhler, P., Guanter, L., Joiner, J., 2015. A Linear Method for the Retrieval of Sun-Induced Chlorophyll Fluorescence from GOME-2 and SCIAMACHY Data. https://doi.org/10.5194/amt-8-2589-2015.
Köhler, P., Behrenfeld, M.J., Landgraf, J., Joiner, J., Magney, T.S., Frankenberg, C., 2020. Global retrievals of solar-induced chlorophyll fluorescence at red wavelengths with TROPOMI. Geophys. Res. Lett. 47, 1–10. https://doi.org/10.1029/2020GL087541.
Kravitz, J., Matthews, M., Bernard, S., Griffith, D., 2020. Application of sentinel 3 OLCI for chl-a retrieval over small inland water targets: successes and challenges. Remote Sens. Environ. 237, 111562. https://doi.org/10.1016/j.rse.2019.111562.
Kritten, L., Preusker, R., Fischer, J., 2020. A New Retrieval of Sun-Induced Chlorophyll Fluorescence in Water from Ocean Colour Measurements Applied on OLCI L-1b and L-2 1–24. https://doi.org/10.3390/rs12233949.
Kutser, T., 2009. Passive optical remote sensing of cyanobacteria and other intense phytoplankton blooms in coastal and inland waters. Int. J. Remote Sens. 30, 4401–4425. https://doi.org/10.1080/01431160802562305.
Kutser, T., Paavel, B., Verpoorter, C., Ligi, M., Soomets, T., Toming, K., Casal, G., 2016. Remote sensing of black lakes and using 810 nm reflectance peak for retrieving water quality parameters of optically complex waters. Remote Sens. 8 https://doi.org/10.3390/rs8060497.
Lee, Z., Jiang, M., Davis, C., Pahlevan, N., Ahn, Y.H., Ma, R., 2012. Impact of multiple satellite ocean color samplings in a day on assessing phytoplankton dynamics. Ocean Sci. J. 47, 323–329. https://doi.org/10.1007/s12601-012-0031-5.
Letelier, R.M., Abbott, M.R., 1996. An analysis of chlorophyll fluorescence algorithms for the moderate resolution imaging spectrometer (MODIS). Remote Sens. Environ. 58, 215–223. https://doi.org/10.1016/S0034-4257(96)00073-9.
Li, Linhai, Li, Lin, Song, K., Li, Y., Tedesco, L.P., Shi, K., Li, Z., 2013. An inversion model for deriving inherent optical properties of inland waters: establishment, validation and application. Remote Sens. Environ. 135, 150–166. doi:https://doi.org/10.1016/j.rse.2013.03.031.
Loizzo, R., Ananasso, C., Guarini, R., Lopinto, E., Candela, L., Pisani, A.R., 2016. The Prisma Hyperspectral Mission. Eur. Sp. Agency, pp. 9–13 (special Publ. ESA SP SP-740).
Lou, X., Hu, C., 2014. Diurnal changes of a harmful algal bloom in the East China Sea: Bservations from GOCI. Remote Sens. Environ. 140, 562–572. https://doi.org/10.1016/j.rse.2013.09.031.
Lu, D., Goebel, J., Qi, Y., Zou, J., Han, X., Gao, Y., Li, Y., 2005. Morphological and genetic study of Prorocentrum donghaiense Lu from the East China Sea, and comparison with some related *Prorocentrum* species. Harmful Algae 4, 493–505. https://doi.org/10.1016/j.hal.2004.08.015.
Maritorena, S., Morel, A., Gentili, B., 2000. Determination of the fluorescence quantum yield by oceanic phytoplankton in their natural habitat. Appl. Opt. 39, 6725–6737. https://doi.org/10.1364/AO.39.006725.
Matthews, M.W., 2011. A current review of empirical procedures of remote sensing in inland and near-coastal transitional waters. Int. J. Remote Sens. 32, 6855–6899. https://doi.org/10.1080/01431161.2010.512947.
Matthews, M.W., Bernard, S., 2013. Using a two-layered sphere model to investigate the impact of gas vacuoles on the inherent optical properties of *Microcystis aeruginosa*. Biogeosciences 10, 8139–8157. https://doi.org/10.5194/bg-10-8139-2013.
Matthews, M.W., Bernard, S., Robertson, L., 2012. Remote sensing of environment an algorithm for detecting trophic status (chlorophyll- a), cyanobacterial-dominance, surface scums and fl oating vegetation in inland and coastal waters. Remote Sens. Environ. 124, 637–652. https://doi.org/10.1016/j.rse.2012.05.032.
Mckee, D., Cunningham, A., Wright, D., Hay, L., 2007. Potential impacts of nonalgal materials on water-leaving Sun induced chlorophyll fluorescence signals in coastal waters. Appl. Opt. 46, 7720–7729. https://doi.org/10.1364/AO.46.007720.
McKibben, S.M., Strutton, P.G., Foley, D.G., Peterson, T.D., White, A.E., 2012. Satellite-based detection and monitoring of phytoplankton blooms along the Oregon coast. J. Geophys. Res. Ocean. 117, 1–12. https://doi.org/10.1029/2012JC008114.
Meroni, M., Busetto, L., Colombo, R., Guanter, L., Moreno, J., Verhoef, W., 2010. Performance of spectral fitting methods for vegetation fluorescence quantification. Remote Sens. Environ. 114, 363–374. https://doi.org/10.1016/j.rse.2009.09.010.
Millie, D.F., Schofield, O.M.E., Kirkpatrick, G.J., Johnsen, G., Evens, T.J., 2002. Using absorbance and fluorescence spectra to discriminate microalgae. Eur. J. Phycol. 37, 313–322. https://doi.org/10.1017/S0967026202003700.
Mohammed, G.H., Colombo, R., Middleton, E.M., Rascher, U., van der Tol, C., Nedbal, L., Goulas, Y., 2019. Remote sensing of solar-induced chlorophyll fluorescence (SIF) in vegetation: 50 years of progress. Remote Sens. Environ. https://doi.org/10.1016/j.rse.2019.04.030. Accepted, 111177.
Montes-Hugo, M.A., Fiorani, L., Marullo, S., Roy, S., Gagné, J.P., Borelli, R., Demers, S., Palucci, A., 2012. A comparison between local and global spaceborne chlorophyll indices in the St. Lawrence Estuary. Remote Sens. 4, 3666–3688. https://doi.org/10.3390/rs4123666.
Moore, T.S., Mouw, C.B., Sullivan, J.M., Twardowski, M.S., Burtner, A.M., Ciochetto, A. B., McFarland, M.N., Nayak, A.R., Paladino, D., Stockley, N.D., Johengen, T.H., Yu, A.W., Ruberg, S., Weidemann, A., 2017. Bio-optical properties of cyanobacteria blooms in western Lake Erie. Front. Mar. Sci. 4, 1–20. https://doi.org/10.3389/fmars.2017.00300.
Morel, A., Antoine, D., Gentili, B., 2002. Bidirectional reflectance of oceanic waters: accounting for Raman emission and varying particle scattering phase function. Appl. Opt. 41, 6289. https://doi.org/10.1364/ao.41.006289.
Moreno-madriñán, M.J., Fischer, A.M., 2013. Performance of the MODIS FLH algorithm in estuarine waters: a multi-year (2003−2010) analysis from Tampa Bay. Florida (USA) 1161. https://doi.org/10.1080/01431161.2013.804227.
Morrison, J.R., 2003. In situ determination of the quantum yield of phytoplankton chlorophyll a fluorescence: a simple algorithm, observations, and a model. Limnol. Oceanogr. 48, 618–631. https://doi.org/10.4319/lo.2003.48.2.0618.
Mouw, C.B., Greb, S., Aurin, D., DiGiacomo, P.M., Lee, Z., Twardowski, M., Binding, C., Hu, C., Ma, R., Moore, T., Moses, W., Craig, S.E., 2015. Aquatic color radiometry remote sensing of coastal and inland waters: challenges and recommendations for future satellite missions. Remote Sens. Environ. 160, 15–30. https://doi.org/10.1016/j.rse.2015.02.001.
Muller-Karger, F.E., Hestir, E., Ade, C., Turpie, K., Roberts, D.A., Siegel, D., Miller, R.J., Humm, D., Izenberg, N., Keller, M., Morgan, F., Frouin, R., Dekker, A.G., Gardner, R., Goodman, J., Schaeffer, B., Franz, B.A., Pahlevan, N., Mannino, A.G., Concha, J.A., Ackleson, S.G., Cavanaugh, K.C., Romanou, A., Tzortziou, M., Boss, E.S., Pavlick, R., Freeman, A., Rousseaux, C.S., Dunne, J., Long, M.C., Klein, E., McKinley, G.A., Goes, J., Letelier, R., Kavanaugh, M., Roffer, M., Bracher, A., Arrigo, K.R., Dierssen, H., Zhang, X., Davis, F.W., Best, B., Guralnick, R., Moisan, J., Sosik, H.M., Kudela, R., Mouw, C.B., Barnard, A.H., Palacios, S., Roesler, C., Drakou, E.G., Appeltans, W., Jetz, W., 2018. Satellite sensor requirements for monitoring essential biodiversity variables of coastal ecosystems. Ecol. Appl. 28, 749–760. https://doi.org/10.1002/eap.1682.
Neville, R.A., Gower, J.F.R., 1977. Passive remote sensing of phytoplankton via chlorophyll alpha fluorescence. J. Geophys. Res. 82, 3487–3493. https://doi.org/10.1029/jc082i024p03487.
Nymark, M., Valle, K.C., Brembu, T., Hancke, K., Winge, P., Andresen, K., Johnsen, G., Bones, A.M., 2009. An integrated analysis of molecular acclimation to high light in the marine diatom *Phaeodactylum tricornutum*. PLoS One 4. https://doi.org/10.1371/journal.pone.0007743.
Odermatt, D., Gitelson, A., Brando, V.E., Schaepman, M., 2012. Review of constituent retrieval in optically deep and complex waters from satellite imagery. Remote Sens. Environ. 118, 116–126. https://doi.org/10.1016/j.rse.2011.11.013.
O'Malley, R.T., Behrenfeld, M.J., Westberry, T.K., Milligan, A.J., Shang, S., Yan, J., 2014. Geostationary satellite observations of dynamic phytoplankton photophysiology. Geophys. Res. Lett. 41, 5052–5059. https://doi.org/10.1002/2014GL060246.
Palacios, S.L., Kudela, R.M., Guild, L.S., Negrey, K.H., Torres-Perez, J., Broughton, J., 2015. Remote sensing of phytoplankton functional types in the coastal ocean from the HyspIRI preparatory Flight campaign. Remote Sens. Environ. 167, 269–280. https://doi.org/10.1016/j.rse.2015.05.014.
Palmer, S.C.J., Odermatt, D., Hunter, P.D., Brockmann, C., Présing, M., Balzter, H., Tóth, V.R., 2015. Satellite remote sensing of phytoplankton phenology in Lake

Balaton using 10years of MERIS observations. Remote Sens. Environ. 158, 441–452. https://doi.org/10.1016/j.rse.2014.11.021.
Popik, A.Y., Gamayunov, E.L., 2015. The dependence of the fluorescence spectrum of phytoplankton on external influences. Pacific Sci. Rev. A Nat. Sci. Eng. 17, 29–33. https://doi.org/10.1016/j.psra.2015.11.004.
Poulin, C., Antoine, D., Huot, Y., 2018. Diurnal variations of the optical properties of phytoplankton in a laboratory experiment and their implication for using inherent optical properties to measure biomass. Opt. Express 26, 711. https://doi.org/10.1364/oe.26.000711.
Qi, L., Lee, Z., Hu, C., Wang, M., 2017. Requirement of minimal signal-to-noise ratios of ocean color sensors and uncertainties of ocean color products. J. Geophys. Res. Ocean. 122, 2595–2611. https://doi.org/10.1002/2016JC012558.
Rascher, U., Alonso, L., Burkart, A., Cilia, C., Cogliati, S., Colombo, R., Damm, A., Drusch, M., Guanter, L., Hanus, J., Hyvärinen, T., Julitta, T., Jussila, J., Kataja, K., Kokkalis, P., Kraft, S., Kraska, T., Matveeva, M., Moreno, J., Muller, O., Panigada, C., Pikl, M., Pinto, F., Prey, L., Pude, R., Rossini, M., Schickling, A., Schurr, U., Schüttemeyer, D., Verrelst, J., Zemek, F., 2015. Sun-induced fluorescence - a new probe of photosynthesis: first maps from the imaging spectrometer HyPlant. Glob. Chang. Biol. 21, 4673–4684. https://doi.org/10.1111/gcb.13017.
Roesler, C.S., Barnard, A.H., 2013. Optical proxy for phytoplankton biomass in the absence of photophysiology: rethinking the absorption line height. Methods Oceanogr. 7, 79–94. https://doi.org/10.1016/j.mio.2013.12.003.
Roesler, C.S., Perry, M.J., 1995. In situ phytoplankton absorption, fluorescence emission, and particulate backscattering spectra determined from reflectance. J. Geophys. Res. 100, 279–294.
Ronald, J., Zaneveld, V., 1982. Remotely sensed reflectance and its dependence on vertical structure: a theoretical derivation. Appl. Opt. 21, 4146–4150.
Ryan, J.P., Davis, C.O., Tufillaro, N.B., Kudela, R.M., Gao, B.C., 2014. Application of the hyperspectral imager for the coastal ocean to phytoplankton ecology studies in Monterey Bay, CA, USA. Rem. Sens. 6, 1007–1025. https://doi.org/10.3390/rs6021007.
Salyuk, P., Bukin, O., Alexanin, A., Pavlov, A., Mayor, A., Shmirko, K., Akmaykin, D., Krikun, V., 2010. Optical properties of Peter the Great Bay waters compared with satellite ocean colour data. Int. J. Remote Sens. 31 (17–18), 4651–4664. https://doi.org/10.1080/01431161.2010.485219.
Schalles, J.F., 2006. Chapter 3 Phytoplankton Chlorophyll A Concentrations in Concentrations Schalles, pp. 27–79.
Simis, S.G.H., Huot, Y., 2012. Optimization of Variable Fluorescence Measurements of Phytoplankton Communities with Cyanobacteria, pp. 13–30. https://doi.org/10.1007/s11120-012-9729-6.
Siswanto, E., Ishizaka, J., Tripathy, S.C., Miyamura, K., 2013. Detection of harmful algal blooms of Karenia mikimotoi using MODIS measurements: a case study of Seto-Inland Sea, Japan. Remote Sens. Environ. 129, 185–196. https://doi.org/10.1016/j.rse.2012.11.003.
Stumpf, R.P., Wynne, T.T., Baker, D.B., Fahnenstiel, G.L., 2012. Interannual variability of cyanobacterial blooms in Lake Erie. PLoS One 7. https://doi.org/10.1371/journal.pone.0042444.
Tenjo, C., Ruiz-Verdú, A., Van Wittenberghe, S., Delegido, J., Moreno, J., 2021. A new algorithm for the retrieval of sun induced chlorophyll fluorescence of water bodies exploiting the detailed spectral shape of water-leaving radiance. Remote Sens. 13, 329 https://doi.org/10.3390/rs13020329.
Tomlinson, M.C., Wynne, T.T., Stumpf, R.P., 2009. An evaluation of remote sensing techniques for enhanced detection of the toxic dinoflagellate, Karenia brevis. Remote Sens. Environ. 113, 598–609. https://doi.org/10.1016/j.rse.2008.11.003.
Tzortziou, M., Herman, J.R., Cede, A., Loughner, C.P., Abuhassan, N., Naik, S., 2015. Spatial and temporal variability of ozone and nitrogen dioxide over a major urban estuarine ecosystem. J. Atmos. Chem. 72, 287–309. https://doi.org/10.1007/s10874-013-9255-8.
Vabson, V., Kuusk, J., Ansko, I., Vendt, R., Alikas, K., Ruddick, K., Ansper, A., Bresciani, M., Burmester, H., Costa, M., D'Alimonte, D., Dall'Olmo, G., Damiri, B., Dinter, T., Giardino, C., Kangro, K., Ligi, M., Paavel, B., Tilstone, G., Van Dommelen, R., Wiegmann, S., Bracher, A., Donlon, C., Casal, T., 2019. Field intercomparison of radiometers used for satellite validation in the 400–900 nm range. Remote Sens. 11. https://doi.org/10.3390/rs11091129.
Wang, M., Son, S.H., Harding, L.W., 2009. Retrieval of diffuse attenuation coefficient in the Chesapeake Bay and turbid ocean regions for satellite ocean color applications. J. Geophys. Res. Ocean. 114, 1–15. https://doi.org/10.1029/2009JC005286.
Wang, W., Li, S., Hashimoto, H., Takenaka, H., Higuchi, A., Kalluri, S., Nemani, R., 2020. An introduction to the geostationary-nasa earth exchange (GeoNEX) products: 1. Top-of-atmosphere reflectance and brightness temperature. Remote Sens. 12, 1–20. https://doi.org/10.3390/RS12081267.
Werdell, P.J., Mcclain, C.R., Goddard, N., Flight, S., States, U., 2019. Satellite Remote Sensing: Ocean Color☆, 3rd ed, Encyclopedia of Ocean Sciences, 3rd edition. Elsevier Ltd. https://doi.org/10.1016/B978-0-12-409548-9.10817-6
Wolanin, A., Rozanov, V.V., Dinter, T., Noël, S., Vountas, M., Burrows, J.P., Bracher, A., 2015. Global retrieval of marine and terrestrial chlorophyll fluorescence at its red peak using hyperspectral top of atmosphere radiance measurements: feasibility study and first results. Remote Sens. Environ. 166, 243–261. https://doi.org/10.1016/j.rse.2015.05.018.
Wynne, T.T., Stumpf, R.P., Briggs, T.O., 2013. Comparing MODIS and MERIS spectral shapes for cyanobacterial bloom detection. Int. J. Remote Sens. 34 (19), 6668–6678. https://doi.org/10.1080/01431161.2013.804228.
Wynne, T.T., Stumpf, R.P., Tomlinson, M.C., Warner, R.A., Tester, P.A., Dyble, J., Fahnenstiel, G.L., 2008. Relating spectral shape to cyanobacterial blooms in the Laurentian Great Lakes. Int. J. Remote Sens. 29, 3665–3672. https://doi.org/10.1080/01431160802007640.
Xing, X.G., Zhao, D.Z., Liu, Y.G., Yang, J.H., Xiu, P., Wang, L., Marine, N., Monitoring, E., 2007. An overview of remote sensing of chlorophyll fluorescence. Ocean Sci. J. 42, 49–59. https://doi.org/10.1007/BF03020910.
Xu, N., Niu, X., Hu, X., Wang, X., Wu, R., Chen, S., Chen, L., Sun, L., Ding, L., Yang, Z., Zhang, P., 2018. Prelaunch calibration and radiometric performance of the advanced MERSI II on FengYun-3D. IEEE Trans. Geosci. Remote Sens. 56, 4866–4875. https://doi.org/10.1109/TGRS.2018.2841827.
Zhao, J., Cao, W., 2012. First attempt to derive chlorophyll-*a* using natural fluorescence in Northern South China Sea. Remote Sens. Lett. 3 (3), 249–258. https://doi.org/10.1080/01431161.2011.566286.
Zhao, D., Xing, X., Liu, Y., Yang, J., Wang, L., 2010. The relation of chlorophyll-a concentration with the reflectance peak near 700 nm in algae-dominated waters and sensitivity of fluorescence algorithms for detecting algal bloom. Int. J. Remote Sens. 31, 39–48. https://doi.org/10.1080/01431160902882512.
Zhou, J., Gilerson, A., Schalles, J., Gross, B., Hlaing, S., Moshary, F., Ahmed, S., Ioannou, I., 2008. Retrieving quantum yield of sun-induced chlorophyll fluorescence near surface from hyperspectral in-situ measurement in productive water. Opt. Express 16, 17468. https://doi.org/10.1364/oe.16.017468.